

UNCLASSIFIED

AD NUMBER

AD838823

LIMITATION CHANGES

TO:

Approved for public release; distribution is unlimited.

FROM:

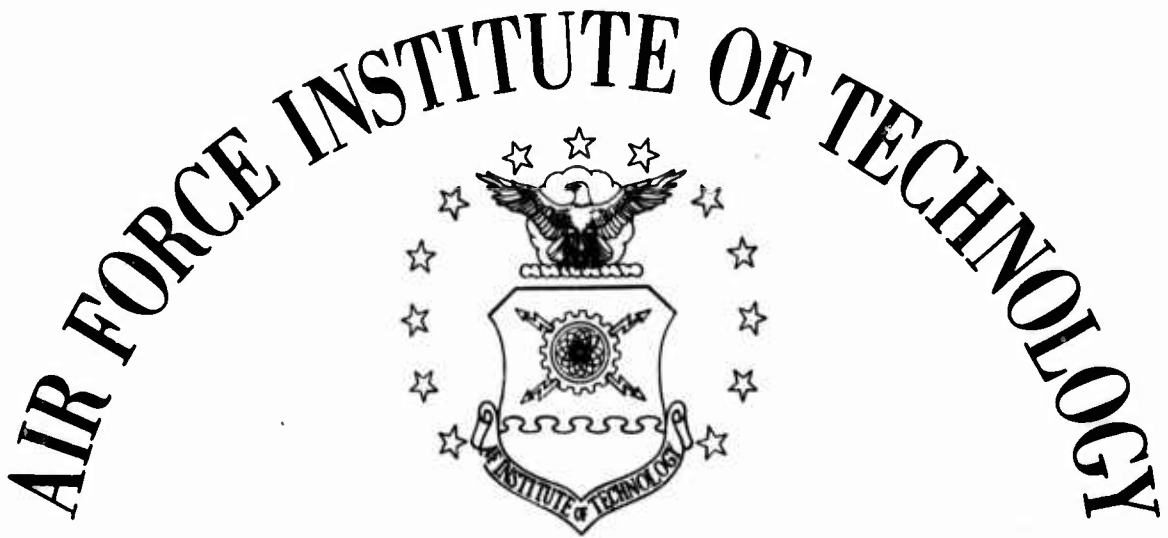
Distribution authorized to U.S. Gov't. agencies and their contractors;
Administrative/Operational Use; JUN 1968. Other requests shall be referred to Air Force Inst of Technology, Wright-Patterson AFB, OH 45433.

AUTHORITY

AFIT ltr 22 Jul 1971

THIS PAGE IS UNCLASSIFIED

AD838823

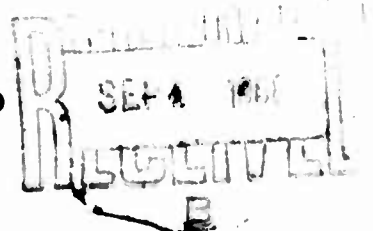


AIR UNIVERSITY
UNITED STATES AIR FORCE



SCHOOL OF ENGINEERING

WRIGHT-PATTERSON AIR FORCE BASE, OHIO



166

f

THESIS

**GAM/AE/68-6 Maurice John William Lehmann
 Captain USAF**

This document is subject to special export controls and each transmittal to foreign governments or foreign nationals may be made only with prior approval of the Dean, School of Engineering, Air Force Institute of Technology (AFIT-SE), Wright-Patterson Air Force Base, Ohio 45433.

GAM/AE/68-6

THE AERODYNAMIC CHARACTERISTICS
OF NON-AERODYNAMIC SHAPES

THESIS

Presented to the Faculty of the School of Engineering of
the Air Force Institution of Technology
Air University
in Partial Fulfillment of the
Requirements for the Degree of
Master of Science

by
Maurice John William Lehmann, B.S.
Captain USAF
Graduate Aerospace-Mechanical Engineering
June 1968

This document is subject to special export controls and each transmittal to foreign governments or foreign nationals may be made only with prior approval of the Dean, School of Engineering, Air Force Institute of Technology (AFIT-SE), Wright-Patterson Air Force Base, Ohio 45433.

Preface

This thesis topic was suggested by Professor Harold Larsen, Head of the Aeronautical Engineering Department at AFIT, to fulfill a request from the Aeronautical Systems Division for wind tunnel data on non-aerodynamic shapes. I would like to thank Squadron Leader Dickinson and Professor Larsen for all their help and guidance during this investigation. The advice and assistance of Mr. A. Barringer, Mr. S. Whitt, and Mr. T. Lokai was greatly appreciated. Mr. D. Norman of ASD also provided valuable suggestions and direction.

Finally, I would like to thank my family for all their help and patience.

Contents

	Page
Preface.	1i
List of Figures.	iv
List of Tables	v
List of Symbols.	vi
Abstract	viii
I. Introduction	1
History	1
Purpose	2
Assumptions and Limitations.	2
II. Apparatus.	3
Wind Tunnel.	3
Balance.	3
Model Mounting System.	6
Models	6
Ultraviolet Light.	7
III. Procedures	9
Calibration of Equipment	9
Model Tests.	10
Data Reduction	11
IV. Accuracy	13
Interference and Tare Effects.	13
Fluorescent-Oil Film Study	15
V. Discussion and Results	19
Rectangles	19
Cylinders.	20
Nose Fairings.	21
VI. Conclusions and Recommendations.	23
Bibliography	25
Appendix A: Tabulated Data	26
Appendix B: Calibration Data	29
Appendix C: Sample Calculations.	41
Appendix D: Graphical Results.	44
Vita	54

List of Figures

Figure		Page
1	AFIT 14-in wind tunnel	4
2	Plexiglas top of test section.	5
3	Wind tunnel control panel and balance read-out panel . .	5
4	Model mounting system.	7
5	Comparison of 2x2x4-in rectangle with 2-1/2 inch elliptical nose fairing and blunt nose model	8
6	Test models.	8
7	Model support used in measuring interference effects . .	10
8	Comparison of center mounting system and top mounting system for 2x2x2-in cube	14
9	Comparison of center mounting system and top mounting system for 2x2x4-in rectangle.	16
10	Oil film studies	18
B.1	Drag tare values for various settings of wind tunnel dynamic pressure (Q)	30
B.2	Lift tare values for various settings of wind tunnel dynamic pressure (Q)	31
B.3	Pitching moment tare values for various settings of wind tunnel dynamic pressure (Q)	31
B.4	Effects of model interference with balance supports on drag tare values.	32
B.5	Calibration of deflection (twist) of 1/4-in rod used as a model mount	33
B.6	Calibration of drag scale.	34
B.7	Calibration of lift scale.	35
B.8	Calibration of pitching moment scale	36
B.9	Calibration of dynamic pressure scale.	37
B.10	Drag coefficient vs angle of attack for cubes of various sizes.	38

Figure		Page
B.11	Lift coefficient vs angle of attack for cubes of various sizes	39
B.12	Pitching moment coefficient vs angle of attack for cubes of various sizes	40
D.1	Drag coefficient vs angle of attack for rectangles at different ratios of side area to frontal area (A_s/A_x).	45
D.2	Lift coefficient vs angle of attack for rectangles at different ratios of side area to frontal area (A_s/A_x).	46
D.3	Pitching moment coefficient vs angle of attack for rectangles at different ratios of side area to frontal area (A_s/A_x)	47
D.4	Drag coefficient vs angle of attack for cylinders at different ratios of projected side area to frontal area (A_s/A_x)	48
D.5	Lift coefficient vs angle of attack for cylinders at different ratios of projected side area to frontal area (A_s/A_x)	49
D.6	Pitching moment coefficient vs angle of attack for cylinders at different ratios of projected side area to frontal area (A_s/A_x)	50
D.7	Effect of different nose fairings on drag of rectangular shape ($A_s/A_x = 2$)	51
D.8	Effect of different nose fairings on lift of rectangular shape ($A_s/A_x = 2$)	52
D.9	Effect of different nose fairings on pitching moment of rectangular shape ($A_s/A_x = 2$)	53

List of Tables

Table		Page
I	Capacity and accuracy of balance	27
II	Test program	28

<u>Symbols</u>	<u>List of Symbols</u> <u>Meaning</u>
A_s	-Model projected side area (in^2)
A_x	-Model frontal area (in^2)
C	-Tunnel test section cross sectional area (in^2)
C	-Degrees Centigrade
C_D	-Drag coefficient
C_L	-Lift coefficient
C_m	-Pitching moment coefficient
D	-Drag (lb)
D_m	-Drag due to model (lb)
D_s	-Drag due to model supports (lb)
e	-Tunnel blockage factor
I_m	-Interference of model on supports
L	-Lift (lb)
L_m	-Lift due to model (lb)
L_s	-Lift due to model supports (lb)
M	-Pitching moment (in-lb)
M_m	-Pitching moment due to model (in-lb)
M_s	-Pitching moment due to model supports (in-lb)
MFA	-Model frontal area (in^2)
P	-Atmospheric pressure (in-hg)
P_o	-Standard sea level atmospheric pressure (29.920 in-hg)
Q	-Corrected tunnel dynamic pressure (lb/ft^2)
Q_u	-Indicated tunnel dynamic pressure (lb/ft^2)
R_n	-Reynolds number
S	-Model frontal area at 0° angle of attack (in^2)

<u>Symbols</u>	<u>Meaning</u>
SFA	-Strut and model mount frontal area (in^2)
T	-Temperature (degrees Kelvin)
T_0	-Standard sea level temperature (288° Kelvin)
V	-Tunnel velocity (ft/sec)
a	-Slope of lift curve
l	-Model length (ft)
α	-Corrected angle of attack (degrees)
α_u	-Indicated angle of attack (degrees)
δ	-Boundary correction factor
μ	-Coefficient of absolute viscosity (lb-sec/ft ²)
ρ	-Density of air (lb-sec ² /ft ⁴)
ρ_0	-Standard sea level density of air (0.002378 lb-sec ² /ft ⁴)
τ_2	-Downwash correction factor

Abstract

A wind tunnel investigation of three basic shapes (cubes, rectangles, and cylinders) was conducted to determine the aerodynamic characteristics of similar shaped cargos carried externally by helicopters or V/STOL aircraft. The ratio of side area to frontal area (A_s/A_x) was used as a parameter to plot the lift, drag, and pitching moment versus angle of attack for the three shapes. All tests were conducted at Reynolds numbers between 10^5 and 10^6 . The aerodynamic characteristics of the rectangles did not vary with Reynolds number. The cylinders, however, were all tested at Reynolds numbers slightly less than critical, and therefore, the cylinder forces in this report will be higher than those obtained at slightly larger Reynolds numbers. The lift, drag, and pitching moment coefficients were plotted for angles of attack from $+5^\circ$ to -90° . The change in slopes of the pitching moment of both rectangles and cylinders was smooth and gradual indicating no rapid changes in static stability. A nose fairing was found to reduce the aerodynamic forces on a rectangle substantially at 0° angle of attack, but increased the forces for angles larger than -45° . By using a very flat nose fairing (i.e. 10% of model length or less) it was possible to reduce the drag by 30% at 0° angle of attack without increasing the forces at the larger angles of attack.

I. Introduction

History

Until recently, helicopter speeds were not high enough to produce large aerodynamic loads on cargo suspended outside the helicopter. With the advent of the rigid rotor helicopter, compound helicopter, and various V/STOL vehicles, which are capable of much higher cruise speeds, aerodynamic forces on the cargo may severely limit the performance of these towing aircraft. These limitations may come from large lift and drag forces or from unstable cargo/sling systems whose fluctuations endanger the towing vehicle.

Previous investigations of non-aerodynamic bodies were mainly concerned with drag. Most of these tests were conducted in the 1920's and 1930's for biplane wing struts and supports as well as for designing automobile shapes. The majority of this data was two-dimensional or, in the case of automobiles, in ground effect. Hoerner's book (Ref 1:3-17) seems to have the most complete data for the drag of these various shaped objects. This reference was used as a basis to check the accuracy of some of the test results.

The Air Force has several missions requiring the transportation of many different cargo configurations. Accurate prediction of range and time required can be obtained only when the effects of the cargo on the towing aircraft's performance are known. To obtain this information Aeronautical Systems Division has requested AFIT to provide wind tunnel data on various cargo configurations. Flight tests have been planned to correlate the wind tunnel results with actual flight conditions (Ref 2).

This study is the initial wind tunnel investigation of the aerodynamic characteristics of non-aerodynamic shapes.

Purpose

The purpose of this investigation is to obtain the lift, drag, and pitching moment characteristics of three basic shapes; cubes, rectangles, and cylinders. The characteristics are plotted versus angle of attack for three ratios of side area to frontal area (A_s/A_x). Area ratio was chosen as a parameter rather than a simple length to width or length to diameter ratio so that more complicated cargo configurations might be approximated by this data.

In addition to the three basic shapes, the effects of different nose fairings on one of the rectangles was investigated. The purpose of this secondary investigation was to determine if any improvement in the aerodynamic characteristics could be obtained.

The final goal of this data is to be able to predict the effects of an external cargo on the performance of the towing vehicle.

Assumptions and Limitations

The assumptions used and the limitations which occurred in this study are as follows:

1. The effect of interference between the model and the balance support was assumed to be small using the procedures outlined in this report.
2. It was assumed that the model mounting system used would give similar characteristics as the full scale cargo.
3. The cylinder tests were limited to Reynolds numbers below the critical Reynolds number due to the maximum capacity of the balance.

II. Apparatus

The equipment used in this investigation consisted of the AFIT fourteen-inch wind tunnel, a pyramidal balance, a model mounting system, and several models of various sizes.

Wind Tunnel

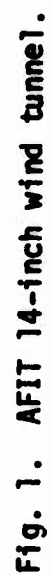
The AFIT 14-in wind tunnel is a single return, closed circuit, tunnel with provisions for 10% air exchange, introduced just prior to the fan. The dimensions and layout of the tunnel are shown in Fig. 1.

The test section is circular and is 32.5-in long. The entrance diameter is 13.875-in and the exit diameter is 14.0-in. This slight divergence allows for the boundary layer growth along the walls of the test section. The top half of the test section is removable to provide access to the model and model mounting system. The top is constructed of clear Plexiglas for observations or photography while the tunnel is in operation (Fig. 2).

The power for the tunnel is provided by a 120 hp electric motor-generator set. It is connected to the tunnel fan by a belt drive system. The tunnel speed is varied from zero to maximum by rheostats on a control panel left of the balance read-out panel (See Fig. 3).

Balance

The balance installed in the AFIT 14-in wind tunnel is a three-degree-of-freedom, null type, pyramidal balance. Lift, drag, and pitching moment are measured; yaw, side force, and rolling moment are restrained. Three automatic beam-balance scales measure the lift, drag, and pitching moment. Tunnel dynamic pressure is measured by a separate, syphon actuated beam balance. Lift, drag, pitching moment, dynamic



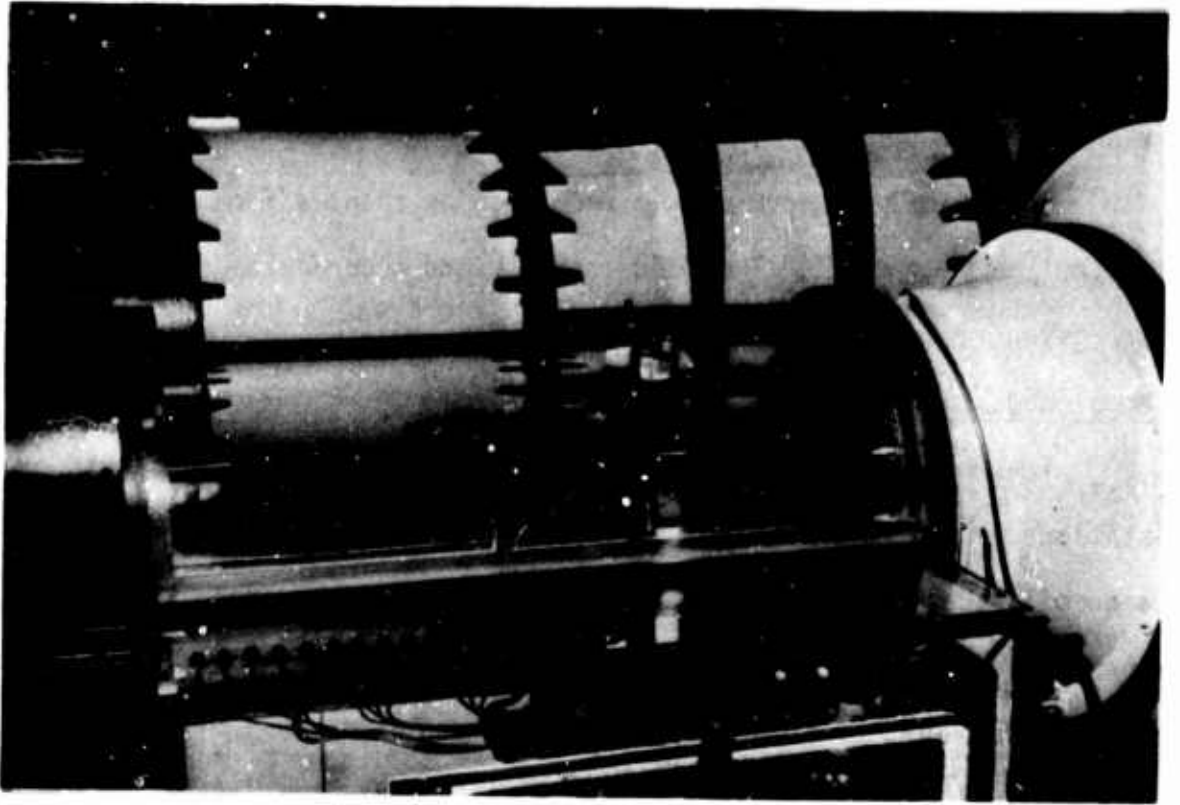


Fig. 2. Plexiglas top of test section.



Fig. 3. Wind tunnel control panel and balance read-out panel.

pressure and balance angle of attack are displayed on a remote balance read-out panel.

The angle of attack of the model can be changed from $\pm 45^\circ$ by a control on this panel. The load capacity and accuracy of each scale are given in Appendix A, Table I.

Model Mounting System

The model is supported by three struts. The front two struts are stationary and the rear strut is movable. Pitching of the model is accomplished by a motor-actuated pitching arm, which moves the rear strut up or down. The pitching arm is controlled by the switch on the balance read-out panel. The front struts are enclosed in fairings to minimize the tare forces and improve the flow characteristics. Dummy fairings are installed in the upper half of the test section as an image system to provide symmetrical flow.

The model is attached to a 1/4-in rod installed between the two front struts. A clamp and bolt arrangement in each model is used for this purpose. A fairing material such as bee's wax is placed in the attachment holes on the model after it is attached to the supporting rod. Two arms at the ends of the rod are connected to the rear support and contain two set screws to fix the angle of attack of the model with respect to the balance angle (Fig. 4). Figure 4 shows the model mounted inverted. This mounting position is explained further in the section on procedures.

Models

The models were constructed by the AFIT shop. The rectangular models were birch, sanded and lacquered. Generally, two inch models of various lengths were used because they were the most compatible to the

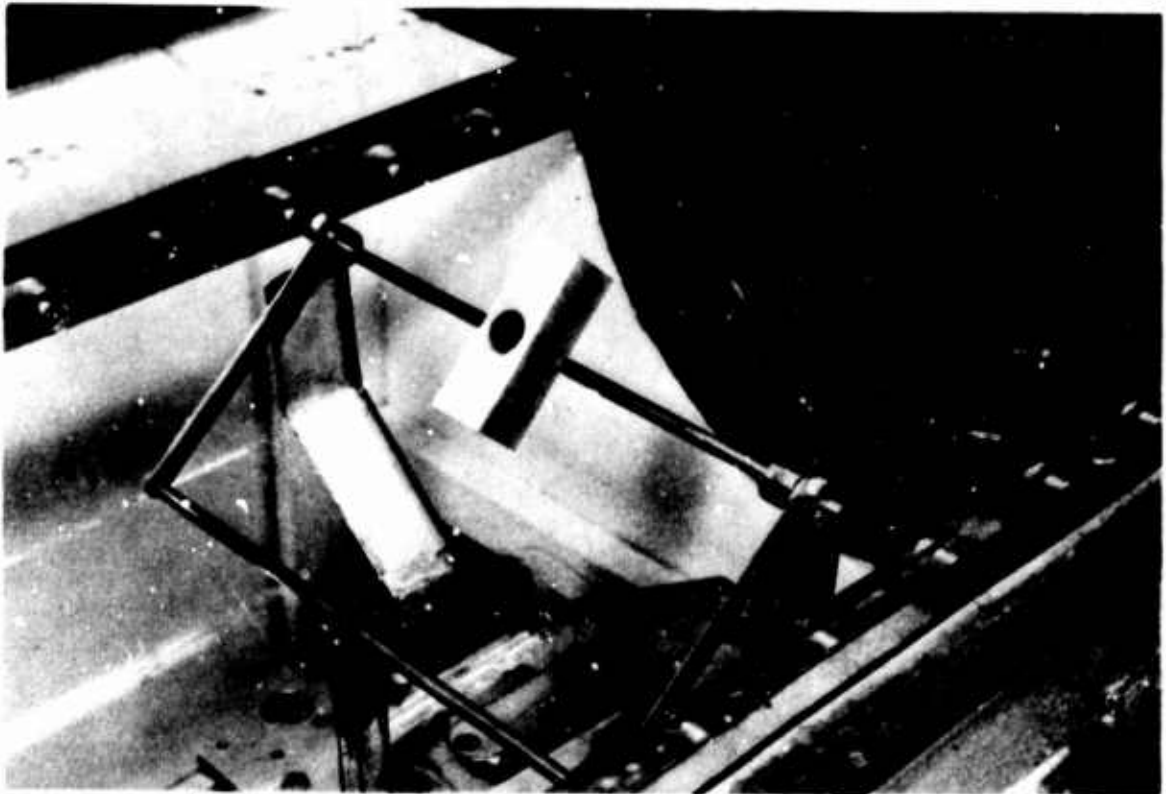


Fig. 4. Model mounting system.

tunnel test section and gave the most consistent results. The nose fairings on the rectangular model were sculptured from bee's wax using a template and pallet knife (Fig. 5).

The cylindrical models were machined from aluminum stock to appropriate dimensions so as to give integer values to the ratio of projected side area to frontal area (A_s/A_x). All models used in this study are shown in Fig. 6.

Ultraviolet Light

Two 100-watt ultraviolet lights were used to obtain fluorescence of oil films on the models. This was used to study the boundary layer and the mounting system interference effects. A short film strip showing the boundary layer on several models is included with this report.

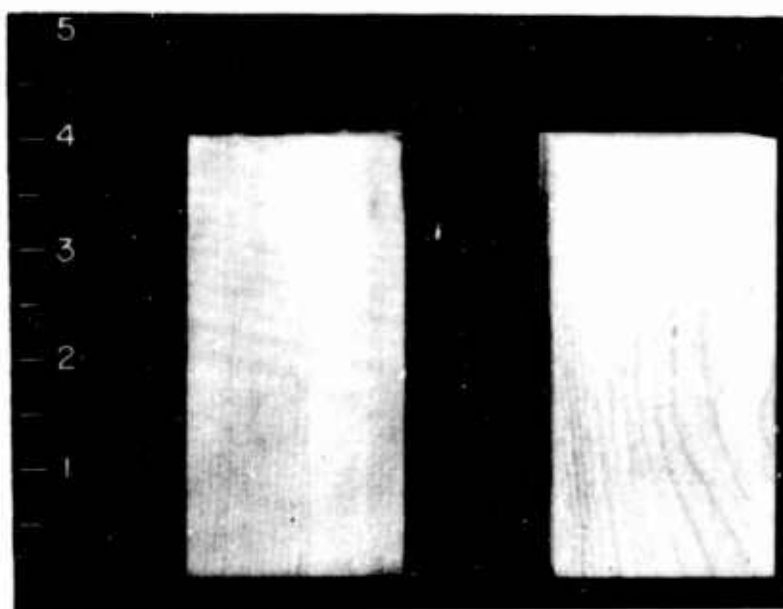


Fig. 5. Comparison of 2x2x4-in rectangle with 2-1/2 inch elliptical nose fairing and blunt nose model.

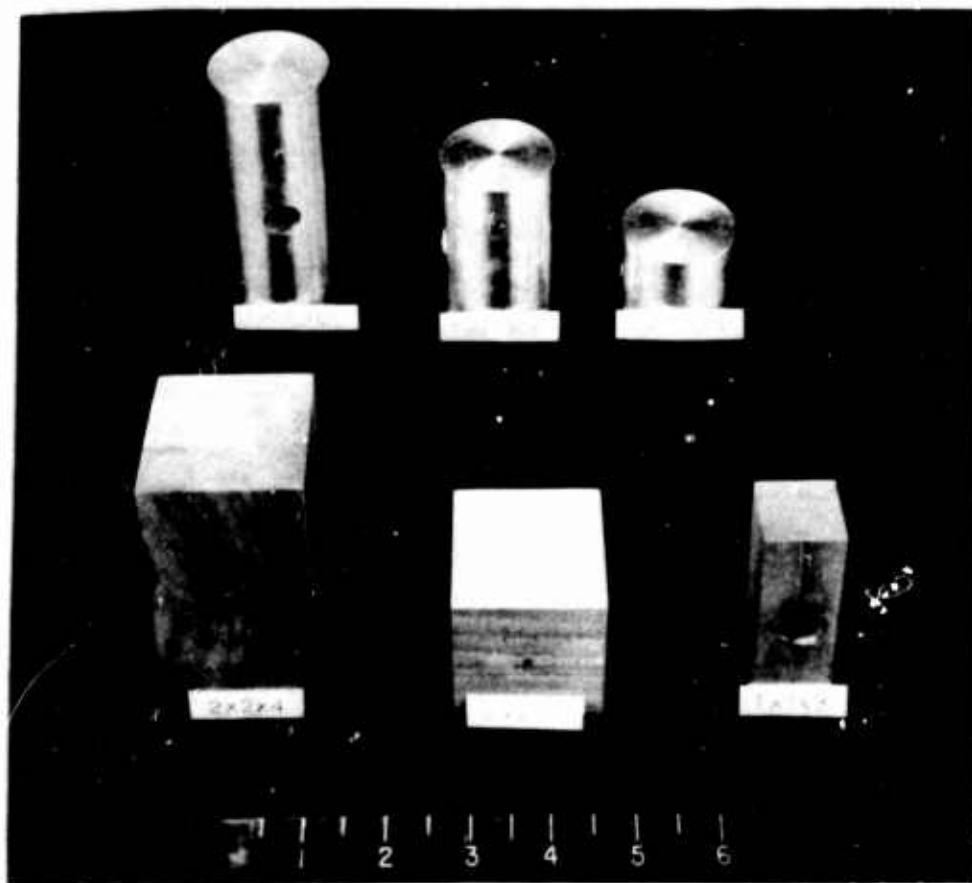


Fig. 6. Test models.

III. Procedures

The procedures used in this investigation were confined to three separate areas; the calibration of equipment, the model tests, and the data reduction.

Calibration of Equipment

Lift, drag, and pitching moment tare values were obtained by installing only the model support system in the tunnel test section. Static readings (i.e. wind off) were recorded for different angles of the balance. Then the forces on the balance were recorded for a given tunnel speed. Finally, static readings were taken after the run and the average of the pre-run and post-run readings were subtracted from the force readings. These data were plotted versus angle of the balance and used as the tare values for the actual tests.

The calibration of the tunnel speed, lift, drag, and pitching moment scales was accomplished by AFIT personnel. The calibration curves are included in Appendix (Fig. B.6-B.9).

When a model is installed in the test section, interference effects between the model and the model support tend to change the tare values. To obtain the magnitude of these effects, a knife edge support was constructed to support the 2x2x2-in cube from the top of the test section (See Fig. 7). This permitted the model to be positioned close to, but not actually touching the model support. Tare runs were made at a tunnel speed of $Q = 50$ psf and with the model at 0° and -90° angle of attack. The tunnel speed was limited to $Q = 50$ psf because of severe lateral vibrations of the model in the -90° position. The interference effects are shown in Fig. B.4. For certain balance

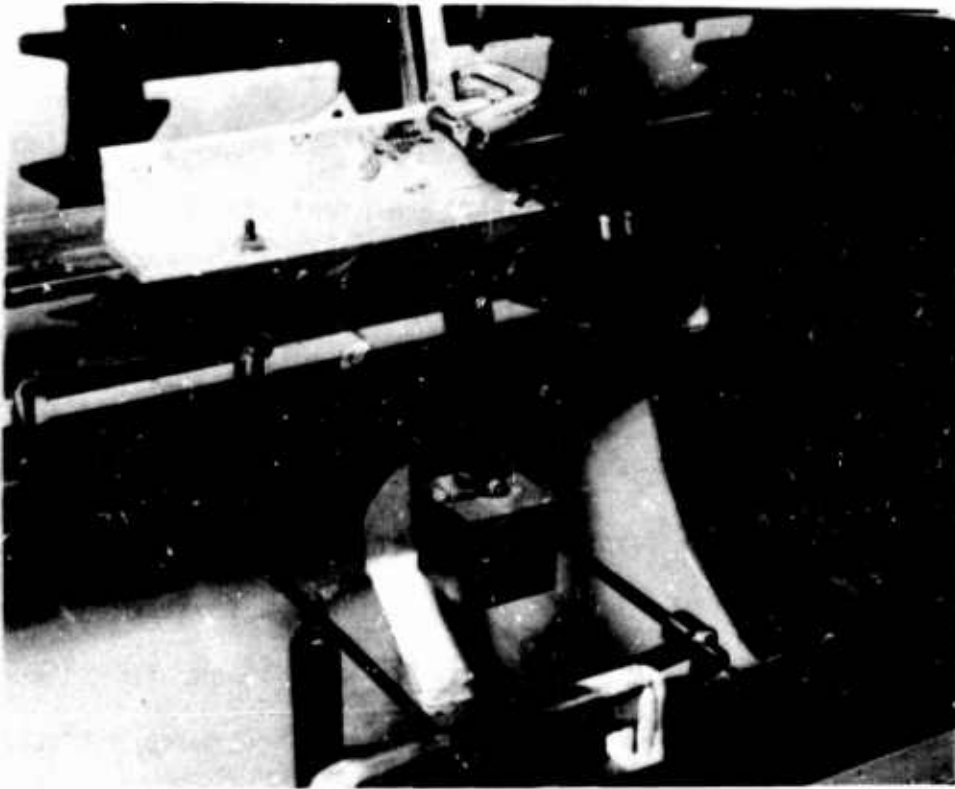


Fig. 7. Model support used in measuring interference effects.

angles, the interference is negligible and to avoid having different tare values for each different model, only these angles were used in the model test procedure.

The amount of deflection (twist) of the 1/4-in rod supporting the model is shown in Appendix B., Figure B.5. Under the loads considered in this study, the deflection was approximately 0.1° . This was less than the accuracy with which the model could be set and was neglected in all the tests.

Model Tests

All the models were mounted in the test section in the inverted position (See Fig. 4). By limiting the balance angle from $+15^\circ$ to $+49^\circ$, the interference effect of the model on the support was minimized. This interference is primarily from the wake of the model impinging on the rear support of the balance, shielding it from the full dynamic

pressure in the test section and resulting in lower tare values. In general, the models were always mounted so the wake passed well above the rear support. Exceptions to this were the longer models at angles of attack from -60° to -90° where it was impossible to keep the wake entirely above the rear support. Slight errors in drag and pitching moment might be expected in these cases.

The models tested were to be rotated from $+5^\circ$ to -90° . A standard routine was used in all the tests. First the balance was set at an angle of $+20^\circ$ and the model mounted inverted at 0° . The top of the test section was secured and static readings were taken at balance angles from $+15^\circ$ to $+49^\circ$. The tunnel speed was set and readings were recorded for the necessary data points. This provided test data for model angles of $+5^\circ$ to -29° . Now the balance was set at 20° and the model remounted at -30° . The above procedure was repeated to obtain test data for model angles of -30° to -59° . This routine was repeated twice more to obtain test data for model angles up to -90° . The tunnel speed was limited by the drag scale capacity for certain models or model configurations. Table II in Appendix A summarizes the test program used in this study.

Data Reduction

The raw data was obtained by subtracting the average static forces found before and after the run from the indicated forces recorded during the run. From this, the tare values were subtracted and the net forces were corrected according to the calibration curves in Appendix B. The tunnel speed (Q) was corrected for solid blockage in the test section. Three-dimensional wind tunnel boundary corrections were checked but found to be negligible in this investigation. All

coefficients were based on the model frontal area at 0° angle of attack.

These procedures are summarized in Pope (Ref 3:337) and are illustrated with sample calculations in Appendix C.

IV. Accuracy

The 2x2x2-in cube was used as a control model for the test. Previously published data for drag of cubes at 0° angle of attack was used as a basis of comparison (Ref 4:32). During the tests, runs on the 2x2x2-in cube were repeated periodically to insure that the calibration and tare values remained constant. Average deviations from the original run are as follows: Lift 0.05 lb, Drag 0.06 lb, Pitching Moment 0.09 in-lb.

The accuracy of the angle of attack setting was within $\pm 1^\circ$ due to the flexibility of the mounting system and the error induced when setting the model angle with the inclinometer.

No indicated change in lift, drag or pitching moment forces was observed when the tunnel speed was changed by ± 0.5 psf, and it was assumed the speed could be set within the accuracy of the other components.

The repeatability of the data for the 2x2x2-in cube indicates the forces measured were within the required accuracy for this test.

Interference and Tare Effects

To determine the effects of model interference with the balance several tests were run on the 2x2x2-in cube. First, it was established that tare value variations could be minimized by limiting the balance angles used in each test (See procedures). Then, possible Reynolds number's effects were investigated using different tunnel speeds and different size cubes.

The drag, lift and pitching moment are shown in Fig. B.10, Fig. B.11, and Fig. B.12, respectively. The forces on the 1x1x1-in

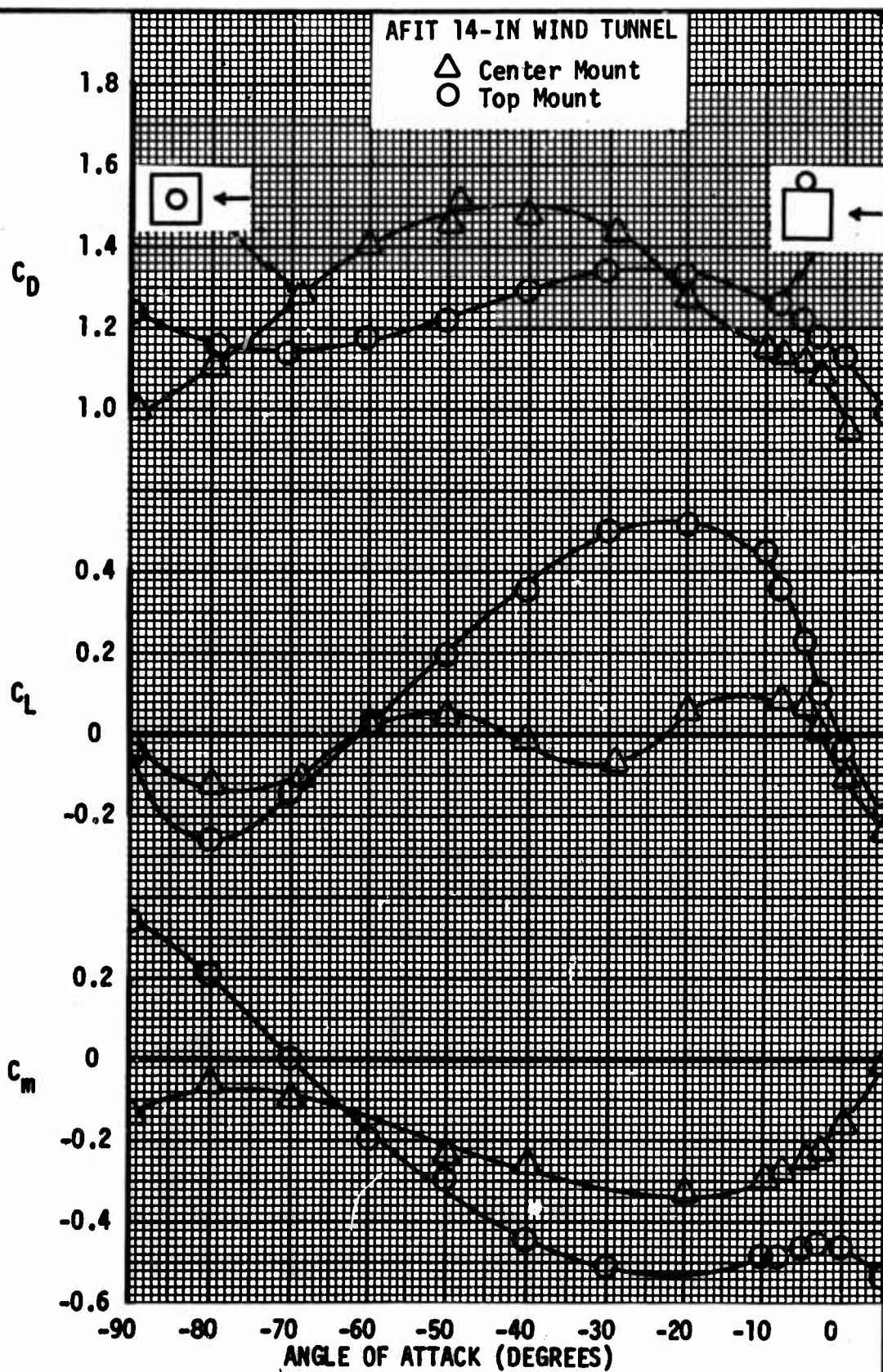


Fig. 8. Comparison of center mounting system and top mounting system for a 2x2x2-in cube.

cube were too small to measure accurately and the data for this model are shown only to indicate that the curve shapes or trends are similar to the two larger models. The data presented were not corrected for the amounts of the support rod covered by each model. A check of several data points using this correction accounts for the difference in the curves of the 2-in cube and the 3-in cube. This indicates there was very little change in the forces with Reynolds number for rectangular shaped objects. This is due to the sharp edges of the model which definitely establishes the separation point regardless of the Reynolds number (Ref 4:31).

The amount of the support rod which is covered or shielded by the model definitely changes the tare values. This was not accounted for in the tests since it is a variable with the angle of attack. The greatest error occurs at -90° where the rod lies in the stagnation area of the leading face of the model.

The support rod mounted on the top of the model also effects the flow around the model. Figure 8 compares the lift, drag and pitching moment of the center mounted cube and the top mounted cube. The tares for the center mounted model were corrected for the shielded portion of the rod. Figure 9 compares the top mounted and center mounted 2x2x4 rectangle. In this case, very little difference is noted except in the magnitude of the pitching moment curve. It is concluded that the top mounted model provides realistic values of the forces for area ratios of 2 or greater.

Fluorescent-Oil Film Study

In order to study the effects of the mounting rod and certain

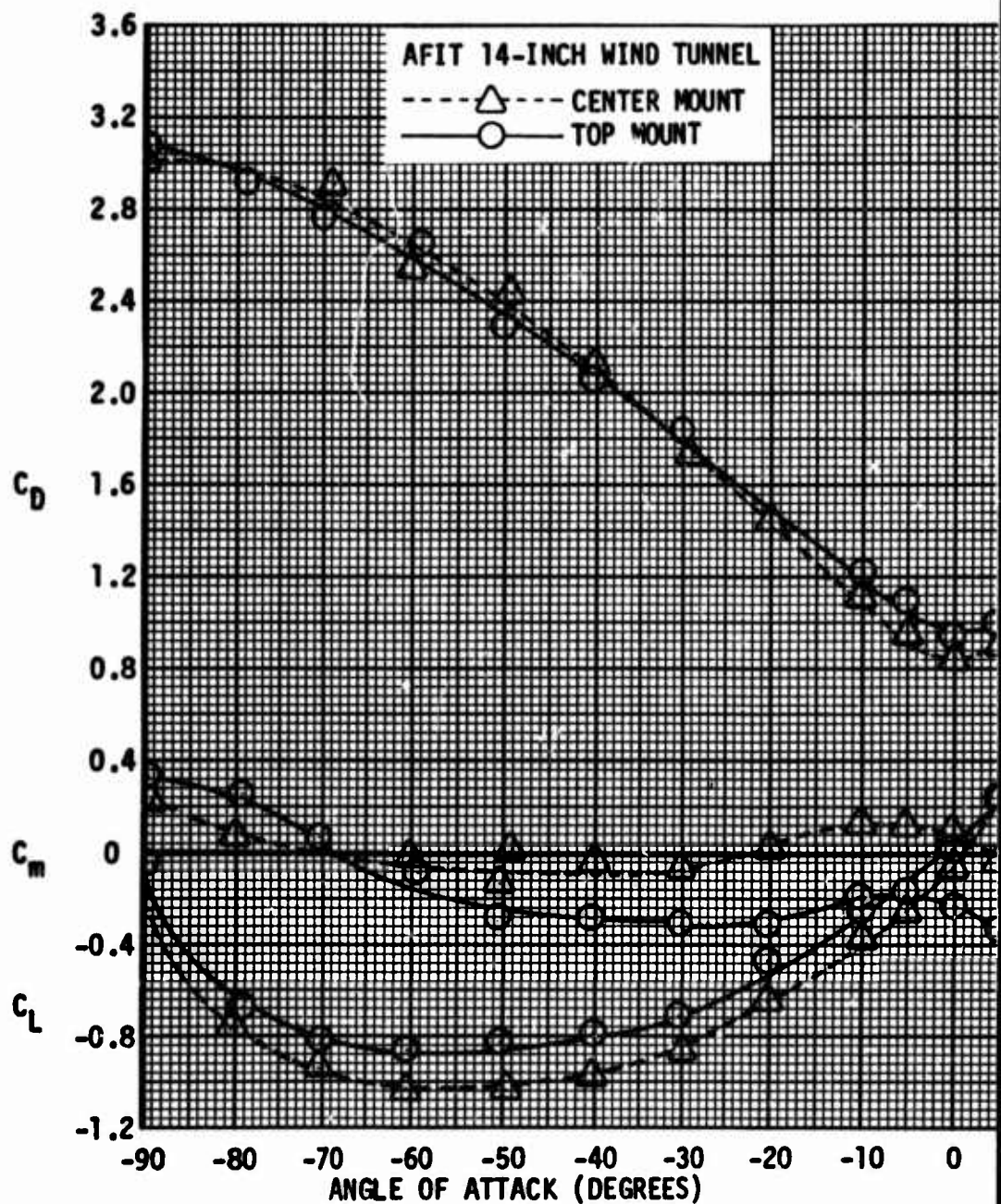


Fig. 9. Comparison of center mounting system and top mounting system for 2x2x4-in rectangle.

flow characteristics, a fluorescent-oil film investigation of several models was made. This technique is based on the fact that ordinary engine oil (SAE 30) is fluorescent under ultraviolet light (Ref 5). The boundary layer action moves the oil film into definite patterns on the surface of the model. These patterns provide qualitative information such as areas of separated flow, areas of reversed flow, and transition points from laminar to turbulent flow. Photographs of several models are shown in Fig. 10.

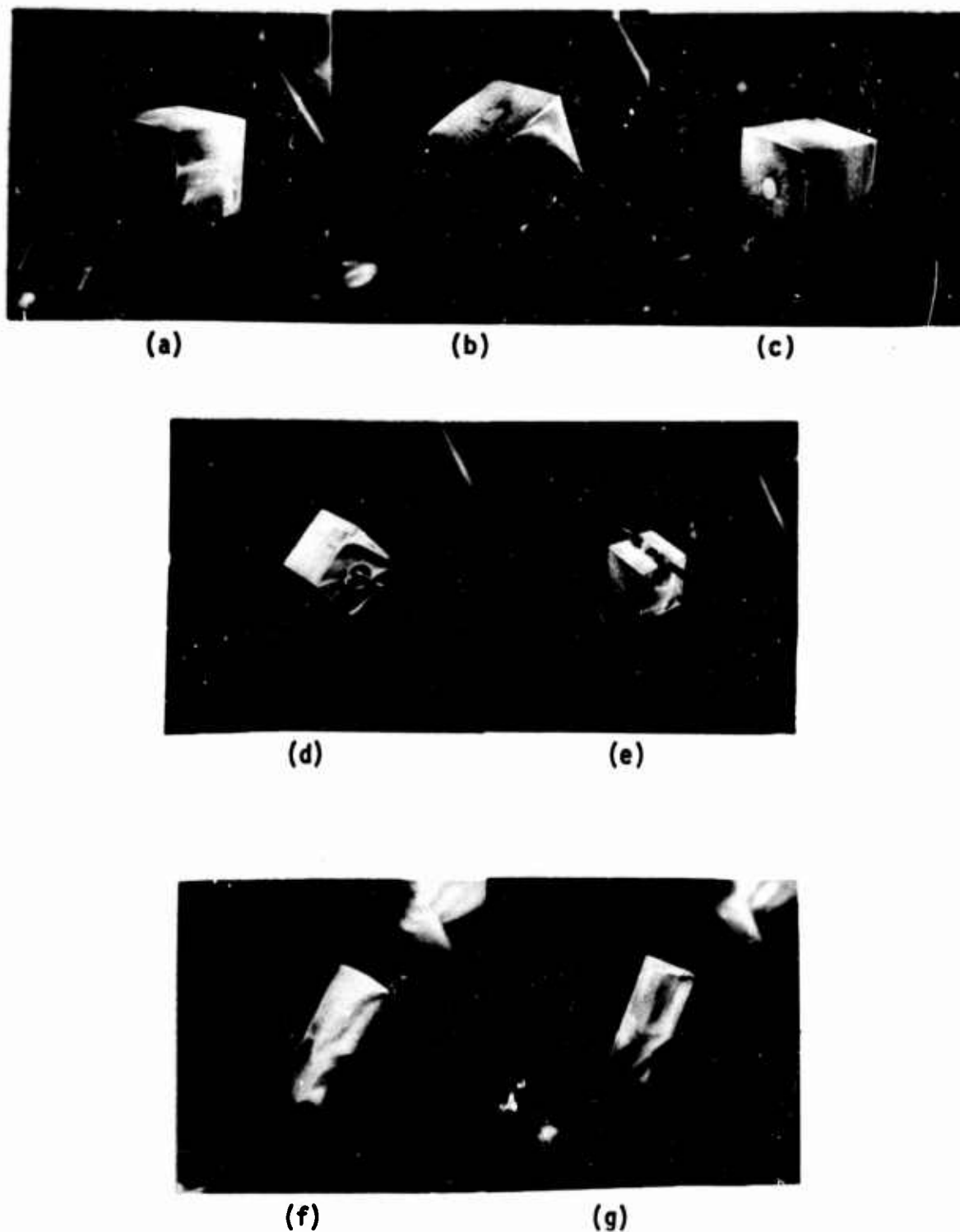


Fig. 10. Oil film studies. Flow from right to left. (a) 3x3x3-in cube at 0°; (b) 3x3x3-in cube at -30°; (c) 3x3x3-in cube at -90°; (d) 2x2x2-in cube with centermount; (e) 2x2x2-in cube with top mount; (f) Cylinder ($A_s/A_x = 3$) at -45°; (g) Cylinder ($A_s/A_x = 3$) at -60°.

V. Discussion of Results

Rectangles

All coefficients in this report are based on the frontal area at 0° angle of attack. The results of the tests have been plotted using a sign convention of nose down moment as negative, and upward force as positive. Since the models were mounted inverted, the signs for the lift and pitching moment data were reversed. Therefore, signs of these forces were changed to correspond to the actual support system as shown in the model sketch at the top of each figure.

The drag curves for rectangles are shown in Fig. D.1. Typically, the curves increase with increasing angle of attack due to the larger profile area exposed to the free stream. The cube is an exception, and shows a decrease in drag for angles of attack greater than -30° . This effect comes from the support interference and a more accurate representation of cube drag was shown previously in Fig. 8. This interference was less noticeable in the higher ratios (A_s/A_x) as confirmed by Fig. 9. Therefore, the data has been presented using the top mounting system since it produced better pitching moment data as well as being more representative of actual support systems.

The lift coefficients for three area ratios are shown in Fig. D.2. In general, the lift decreased from zero until reaching an angle of attack between -40° and -60° where it increases back to zero at -90° . The cube is again an exception due to the support interference. Fig. 8 again shows that cube lift remains essentially zero through the angle of attack range of 0° to -90° . The variations around zero are caused by inaccuracies in measuring very small forces and reducing them to

non-dimensional or coefficient form.

The pitching moment coefficients are shown in Fig. D.3.

Negative slopes occur for area ratios at all angles of attack less than -30° . Positive slopes occur from -5° to -30° but the slope changes are smooth and gradual and do not indicate rapid stability change in this range.

Cylinders

The flow patterns on the cylinder are considerably more complex due to the transverse flow at angles of attack other than zero. Calculations of the Reynolds number for the cylinder model indicated the tests were being conducted very near the critical Reynolds number or transition region (Ref 6:250). A flow visualization study was conducted using the fluorescent-oil film technique. This indicated that laminar flow existed up to tunnel speeds of $Q = 50$ psf. In other words, the tests were conducted at Reynolds numbers slightly less than the critical Reynolds number. It is well known that a decrease in cylinder drag occurs after transition to turbulent flow due to the delay in flow separation. While it would have been desirable to test the cylinders at these higher Reynolds numbers, the size of the test section and the capacity of the balance limited the Reynolds number obtained to less than critical. However, this data should be useful in predicting trends of the lift, drag, and pitching moment at higher Reynolds numbers.

The cylinder drag coefficients are shown in Fig. D.4., and agree with those published by Hoerner (Ref 1, 3-12) at 0° angle of attack. The cylinder drag initially increases with decreasing angles of attack, reaching a peak which is a function of the projected side

area to frontal area ratio. The larger the area ratio, the more negative angle of attack is required for the drag to peak. The decrease in drag at the larger negative angles is due to the lessened drag for the rounded sides of the cylinder as compared to the blunt face of the cylinder.

The cylinder lift varies largely with the area ratio. The lifting force produced by a cylinder at negative angles of attack is the result of the positive force produced by the blunt face at a positive angle of attack and the negative force produced by the sides of the cylinder which are at negative angles of attack. For area ratios of one, the force from the blunt face predominates resulting in a positive lift force. At area ratios of two, the forces are approximately balanced and the resultant force is very nearly zero. At a larger area ratios, the forces on the sides of the cylinder are greater and produce negative resultant forces.

The pitching moment produced by the cylinder is similar to that of the rectangle as shown in Fig. D.6. All area ratios have negative slopes after -30° angle of attack. The slopes from -30° to 0° are slightly positive or zero, but the changes are smooth and gradual indicating no rapid or radical changes in pitching stability.

Nose Fairings

Three different nose fairings were tested on the 2x2x4 rectangle to determine their effects on the aerodynamic characteristics. They are compared with the blunt rectangle to illustrate the magnitude of the changes.

The drag coefficients are shown in Fig. D.7. The hemisphere

and 2-in ellipse fairing produce almost identical drag coefficients and show a decrease in drag of over 50% at zero degrees angle of attack. However, this advantage decreases as the angle of attack becomes more negative, until at -45° the drag becomes greater than the blunt body due to the increased profile area produced by the fairings. The 2-1/2 inch elliptical nose fairing reduced the drag at 0° angle of attack by 30%. This fairing also reduced the drag below the blunt body values up to angles of attack of -70° where it retained approximately the same drag coefficient as the blunt body up to -90° .

All the fairings produced increased negative lift coefficients as shown in Fig. D.8. The magnitudes of these increases are a function of the increased profile area attributed to the fairing.

The pitching moments have positive slopes from 0° to -40° and negative slopes from -40° to -90° as shown in Fig. D.9. Larger values of pitching moment occur for longer nose fairings. Again, the slope changes appear to be smooth and gradual indicating no rapid changes in static stability.

VI. Conclusions and Recommendations

In establishing the aerodynamic characteristics of rectangular and cylindrical shapes, the following conclusions were reached:

1. Reynolds number effects were negligible for rectangular shapes. This was a result of the flow visualization studies and a comparison of force data of the 2x2x2-in cube and the 3x3x3-in cube. The cylinders, of course, are definitely affected by Reynolds number and the values shown in this report would be expected to be less for slightly higher Reynolds numbers.
2. The support interference was difficult to measure and eliminate. It was most apparent on the small models and those with low area ratios. For area ratios of two or greater, the top mounted support gives the best results since it corresponds to the actual support system. For smaller area ratios, errors in the lift and drag forces dictate a center type mounting. This changes the magnitude of the pitching moment, but the slopes of the pitching moment curve remain essentially the same.
3. A rounded nose fairing reduced the drag by a significant amount at low angles of attack, but tended to increase the drag at angles of attack larger than -45° . It was determined that a flat fairing which does not increase the length of the cargo by more than 5% to 10% will result in a substantial decrease in drag at small angles of attack without producing an increase in drag at the larger angles of attack.

To further substantiate the data in this report, it is recommended

that a representative model be tested in the AFIT five foot wind tunnel. The larger test section and wire-type balance should establish any error produced by the original support system. It is recommended that several similar fairings be tested as a tail fairing on the 2x2x4-in rectangle to determine whether the nose fairing or the tail fairing is the most advantageous. The cumulative effect of using both nose and tail fairings could also be assessed.

References

1. Hoerner, Sighard F. Fluid-Dynamic Drag. Published by Author, 1965.
2. Performance Branch (SEFDP). Test Plan For External Cargo Performance Testing of the CH-3C Helicopter. Wright-Patterson Air Force Base, Ohio: Aeronautical Systems Division. March 1967.
3. Pope, Alan. Wind-Tunnel Testing. (Second Edition). New York: John Wiley and Sons, Inc., 1954.
4. McCormick, Barnes W., Jr. Aerodynamics of V/STOL Flight. New York: Academic Press, 1967.
5. Loving, Donald L. and S. Katzoff. The Fluorescent-Oil Film Method and Other Techniques for Boundary-Layer Flow Visualization. NASA Memorandum No. 3-17-59L. National Aeronautics and Space Administration, March 1959.
6. Giles, Ranald V. Theory and Problems of Hydraulics and Fluid Mechanics. New York: Schaum Publishing Co. 1956.
7. Asch Equipment Company. Instruction and Operating Manual for AFIT Wind Tunnel Balance. Asch Equipment Company. January 1951.

Appendix A

In table I, the capacity and accuracy of the AFIT 14-in wind tunnel is shown. Table II summarizes the test program showing model sizes, configurations, etc.

Table I. Capacity and Accuracy of Balance (Ref 7)

LOAD	CAPACITY	REQUIRED ACCURACY
Lift	+ 50 lbs - 25 lbs	± 0.05 lb
Drag	± 10 lbs	± 0.01 lb
Pitching Moment	± 30 lbs	± 0.05 in-lb
Dynamic Pressure	500 lb/ft ²	± 0.5 lb/ft ²
Angle of Attack	$\pm 50^\circ$	0.1°

Table II. Test Program

MODEL	A_s/A_x	ANGLE OF ATTACK RANGE (deg)	TUNNEL SPEED Q (psf)	REYNOLDS NUMBER
2x2x2-in rec.	1	+5 to -90	50	213,000
2x2x4-in rec.	2	+5 to -90	35	356,000
1x1x3-in rec.	3	+5 to -90	50	316,000
1.95x1.54-in cyl.	1	+5 to -90	50	162,000
1.95x3.08-in cyl.	2	+5 to -90	50	321,000
1.95x4.59-in cyl.	3	+5 to -90	50	489,000
2x2x4-in rec. 2-1/2 in 45° elliptical nose	2	+5 to -90	35	356,000
2x2x4-in rec. 2-in 45° elliptical nose	2	+5 to -90	35	356,000
2x2x4-in rec. 2-in dia. hemisphere nose	2	+5 to -90	35	356,000

Appendix B

This appendix contains all the wind tunnel calibrations used in this investigation. In addition, several figures illustrate the interference and Reynolds number effects discovered during the tests.

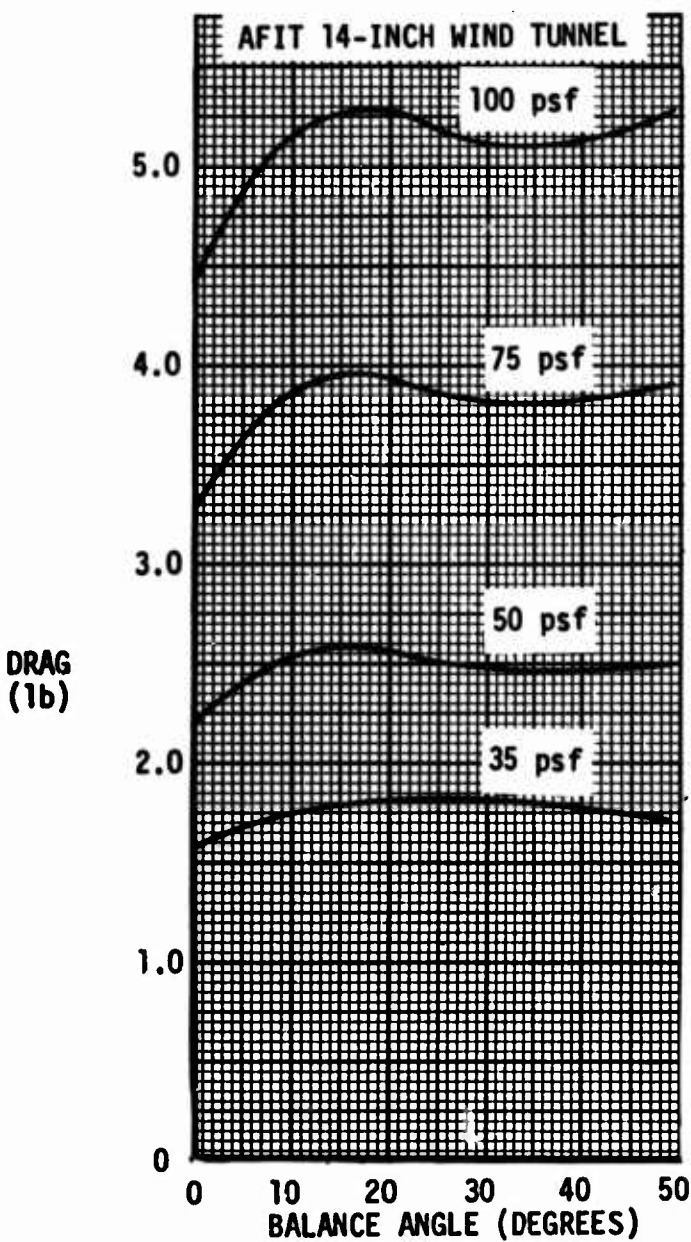


Fig. B.1. Drag tare values for various settings of wind tunnel dynamic pressure (Q).

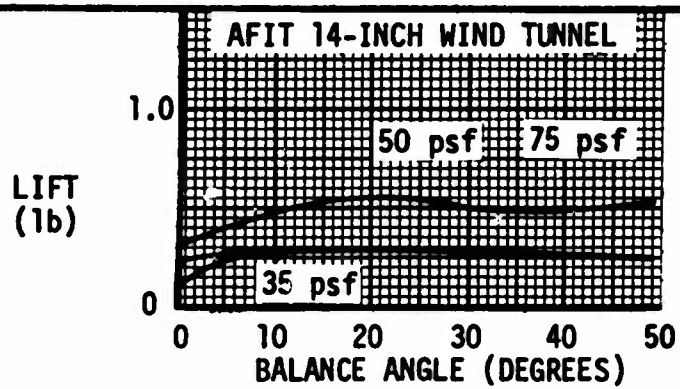


Fig. B.2. Lift tare values for various settings of wind tunnel dynamic pressure (Q).

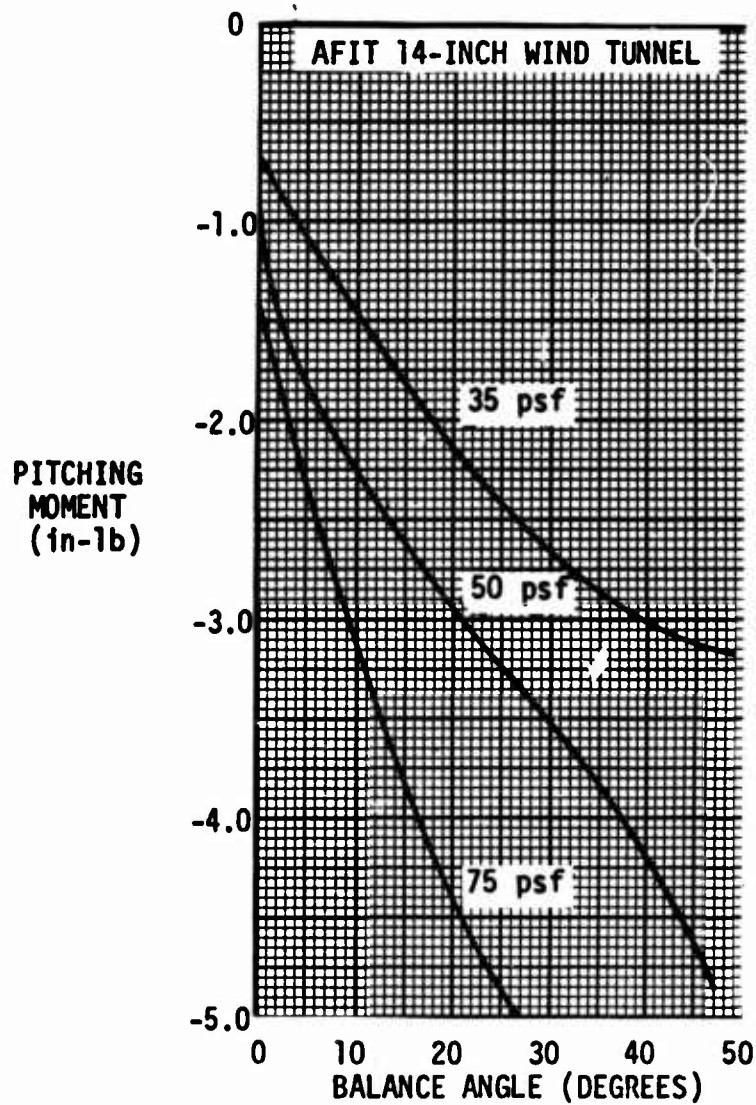


Fig. B.3. Pitching moment tare values for various settings of wind tunnel dynamic pressure (Q).

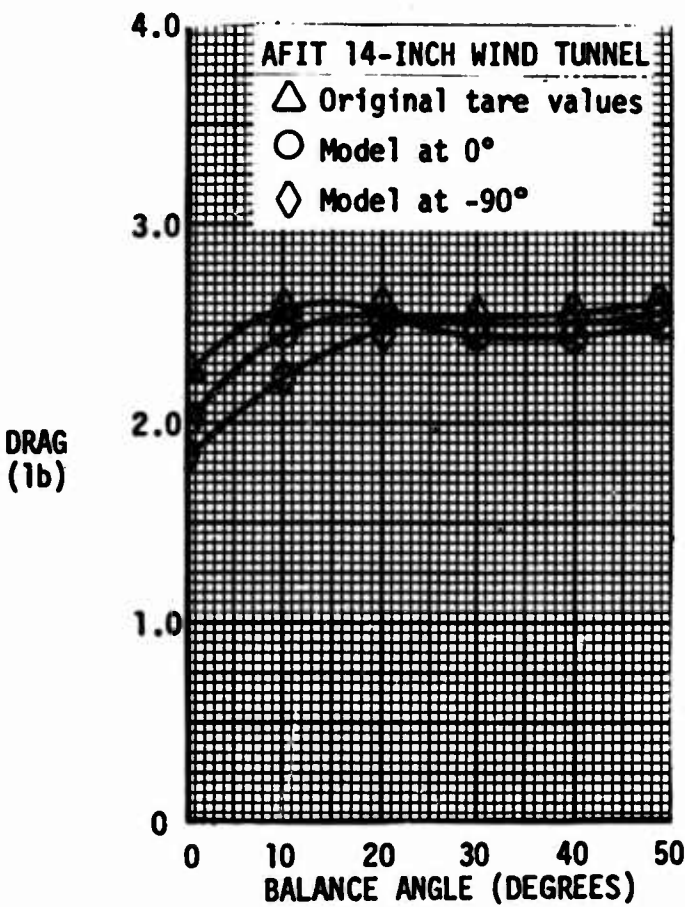
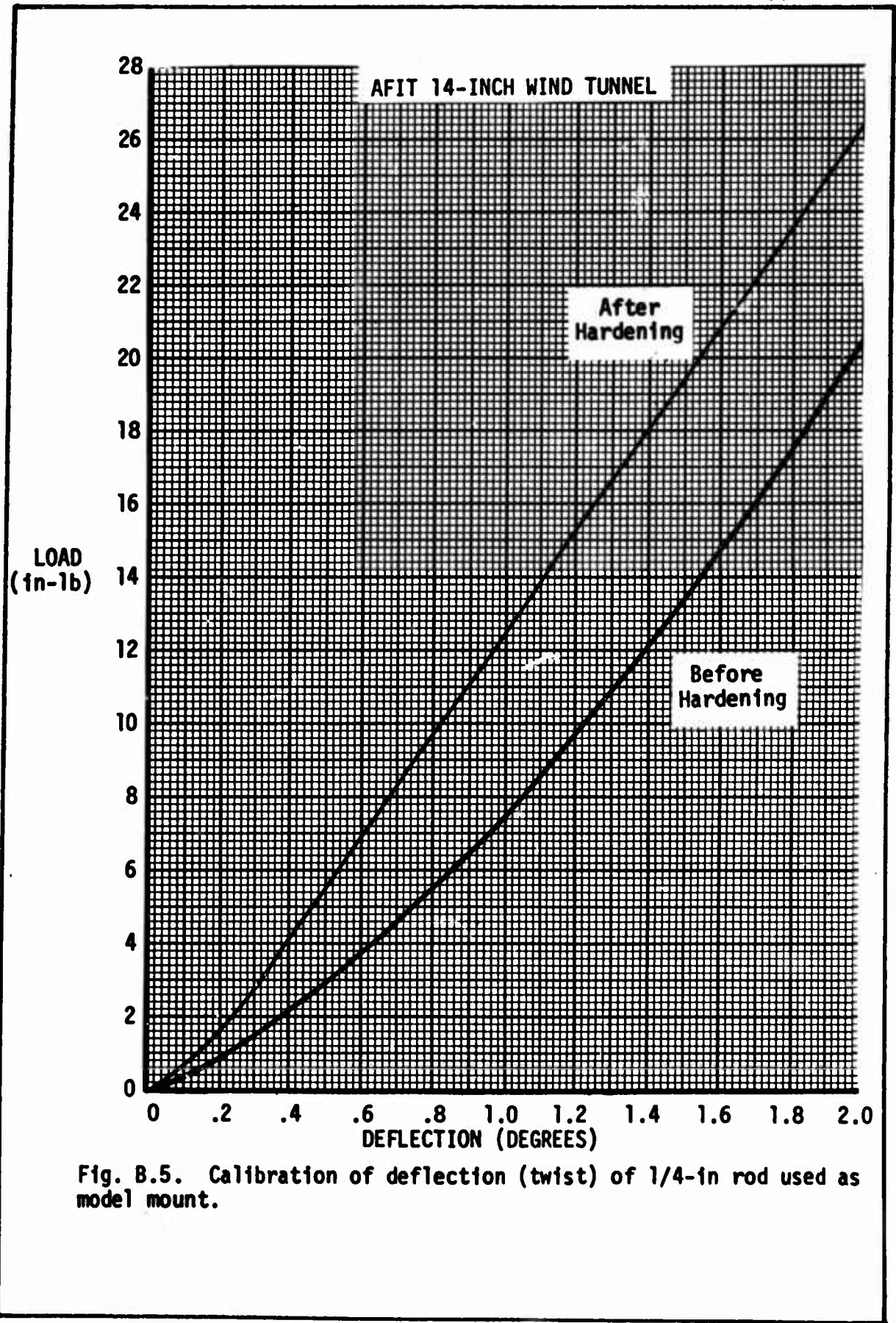


Fig. B.4. Effects of model interference with balance supports on drag tare values.



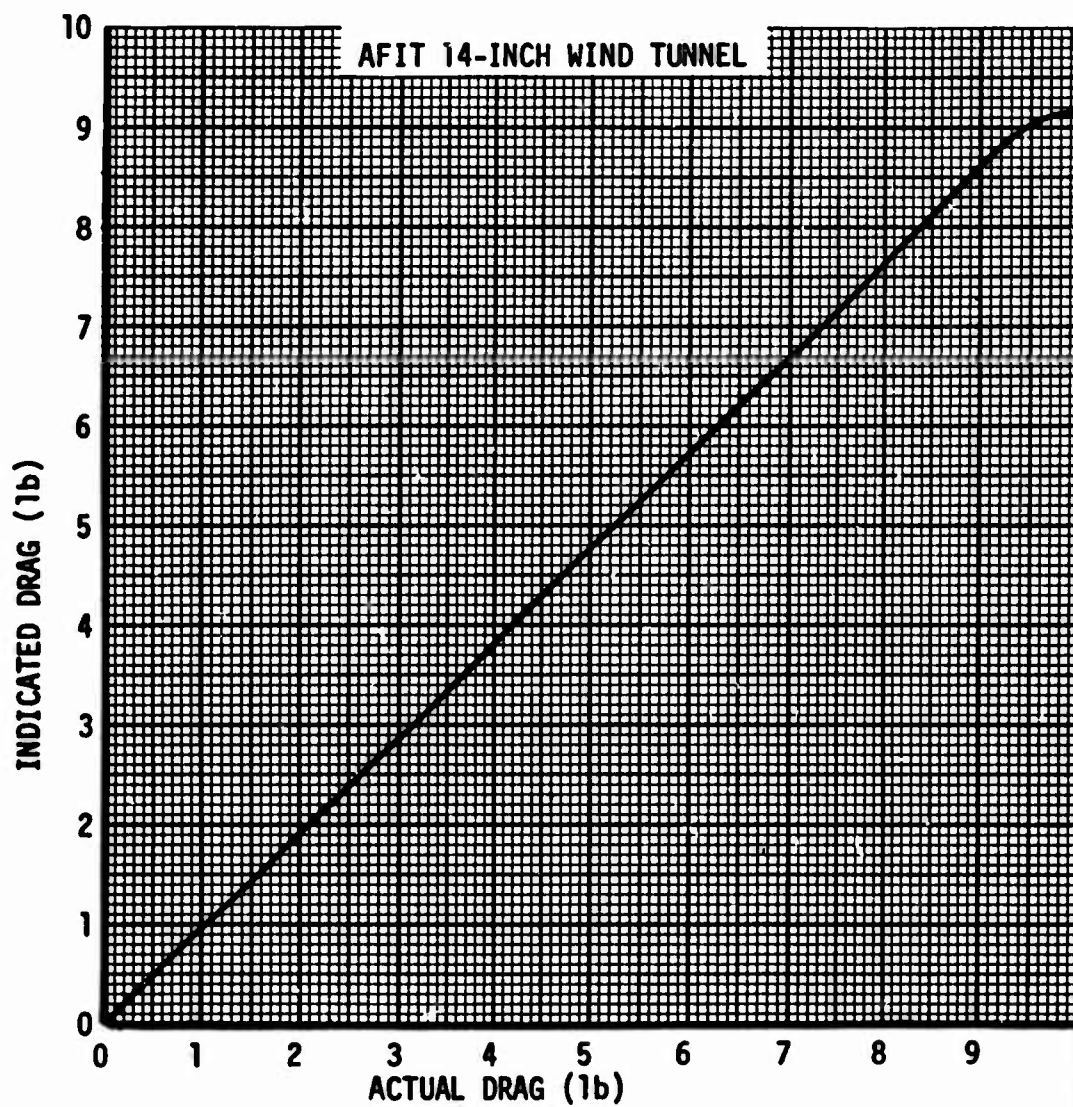


Fig. B.6. Calibration of drag scale.

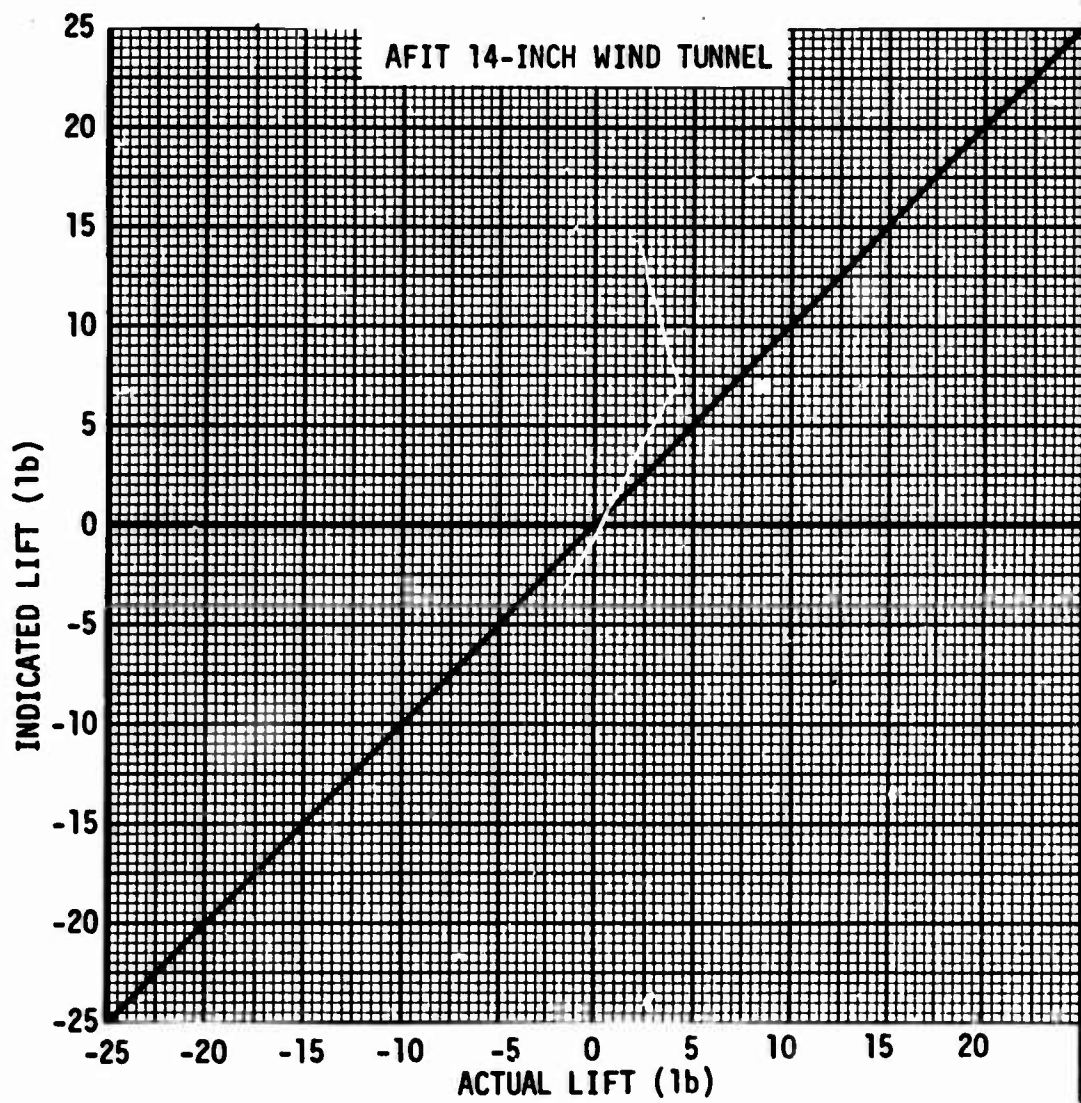


Fig. B.7. Calibration of lift scale.

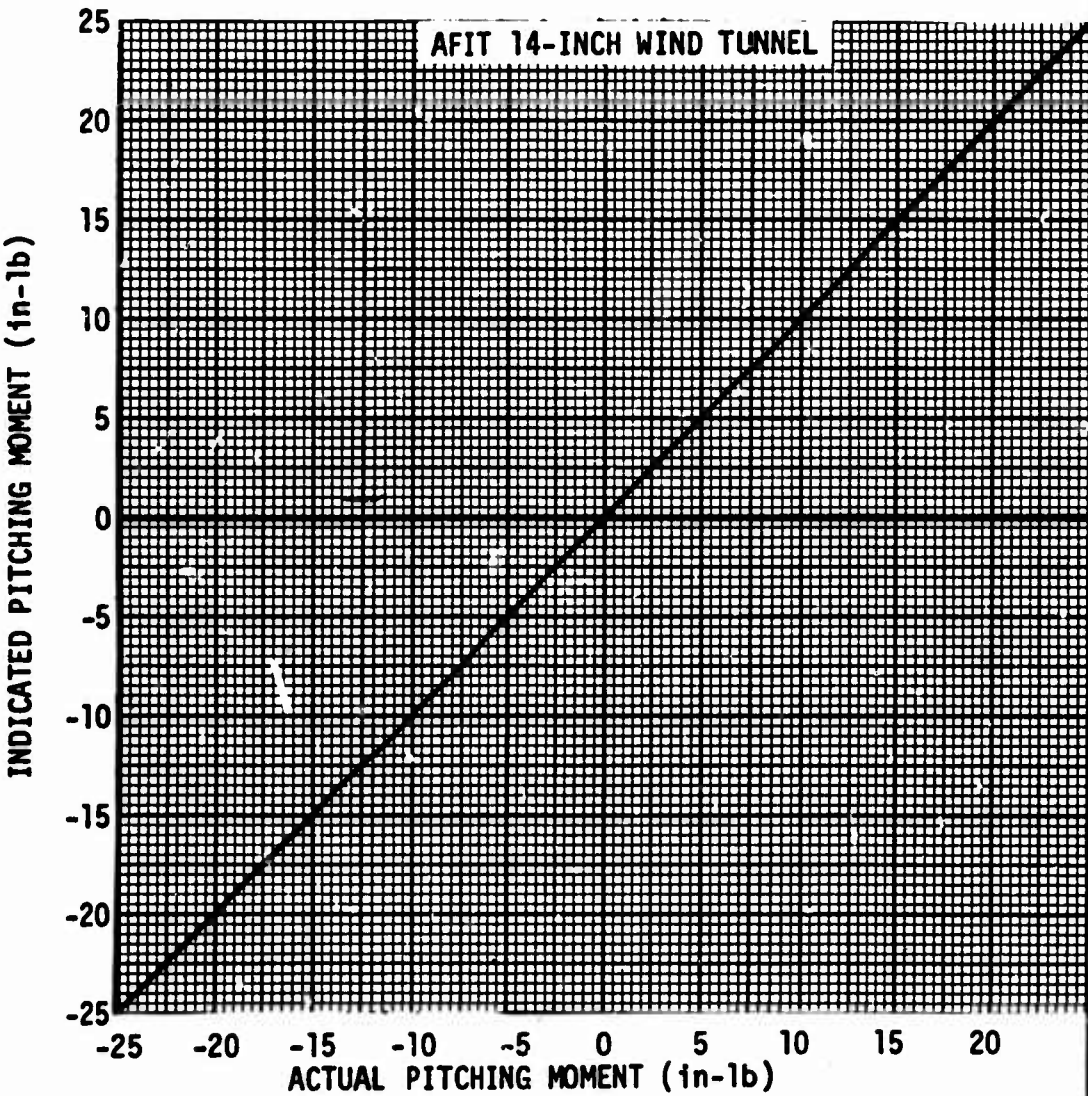


Fig. B.8. Calibration of pitching moment scale.

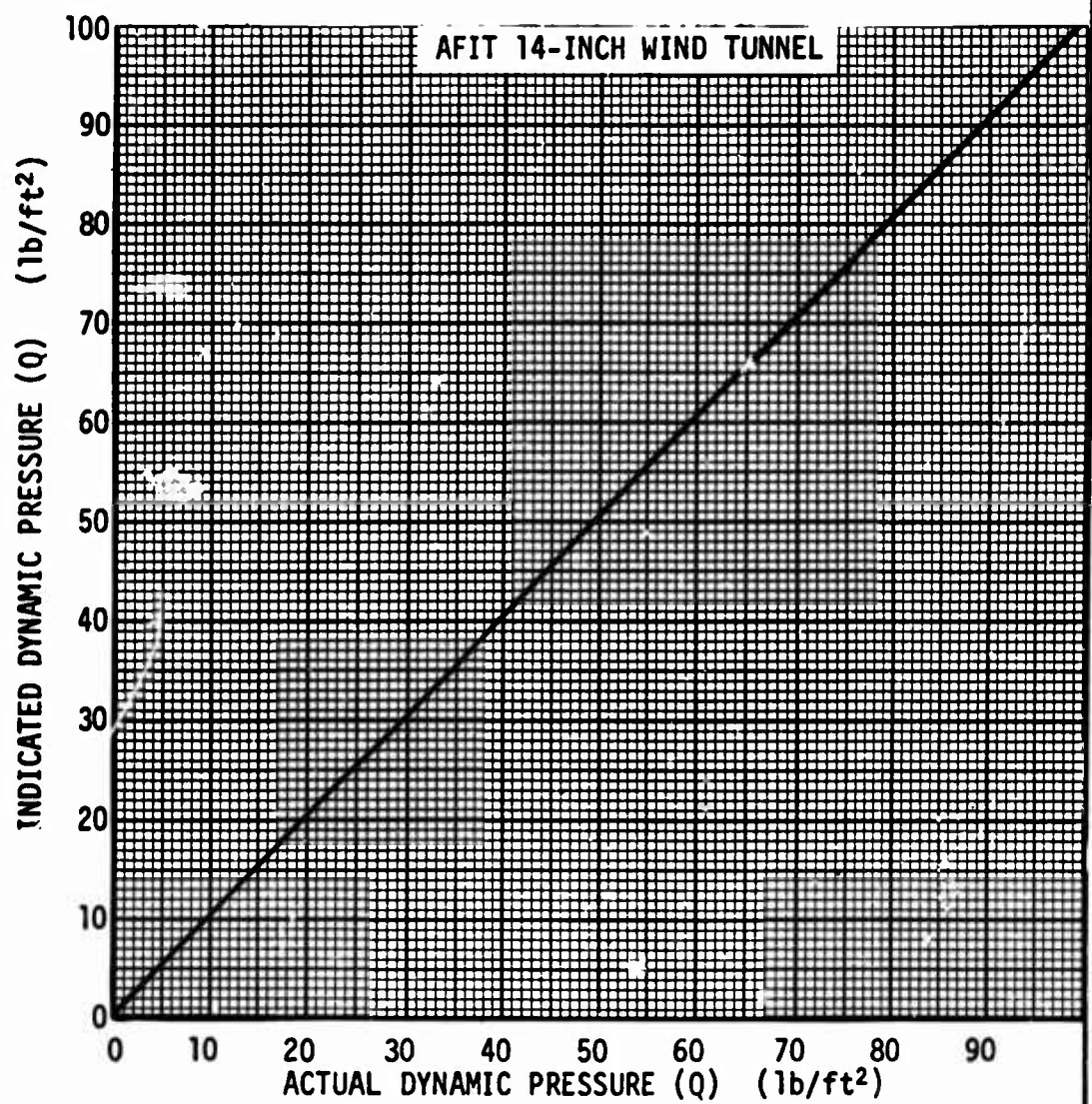


Fig. B.9. Calibration of dynamic pressure scale.

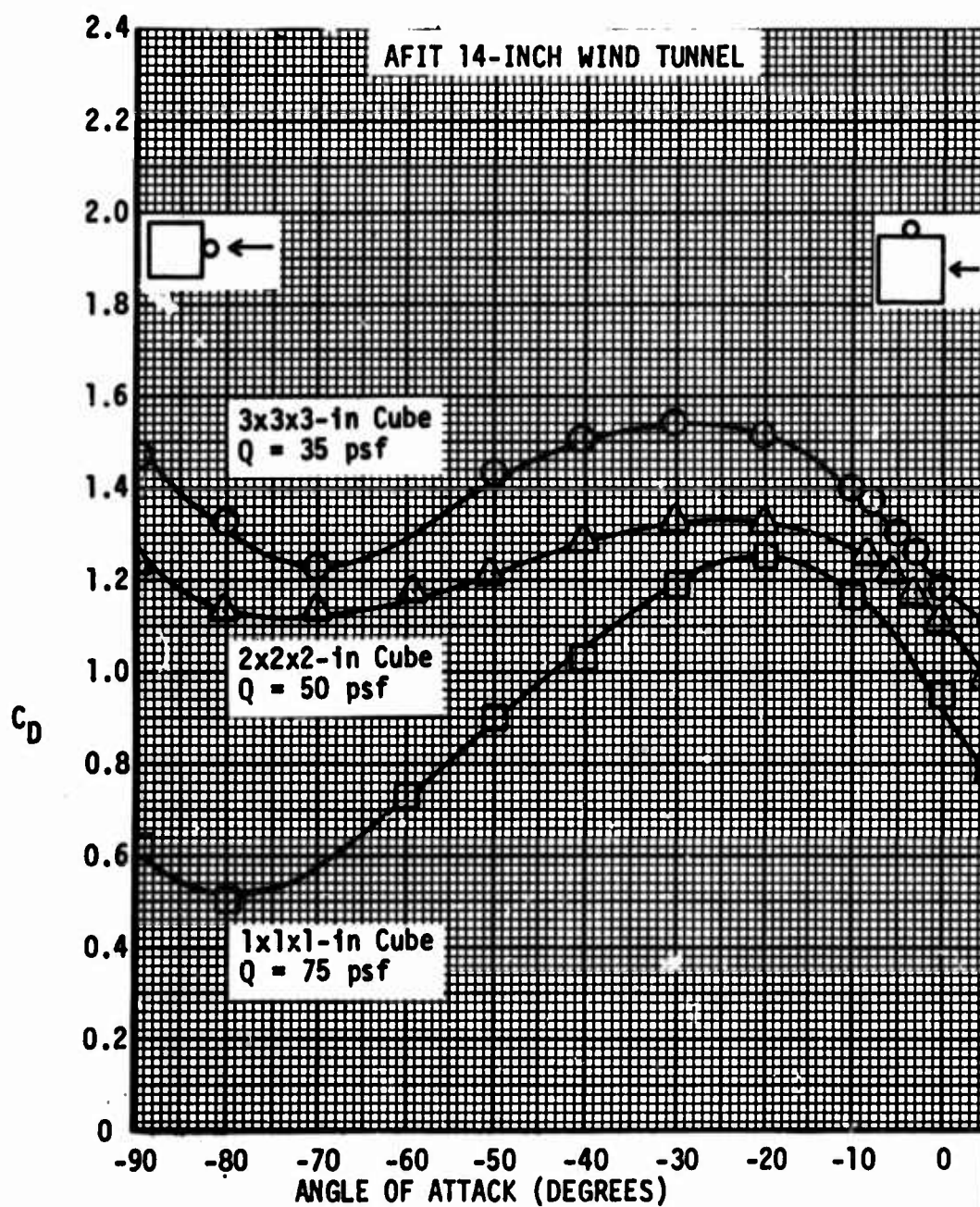


Fig. B.10. Drag coefficient vs angle of attack for cubes of various sizes.

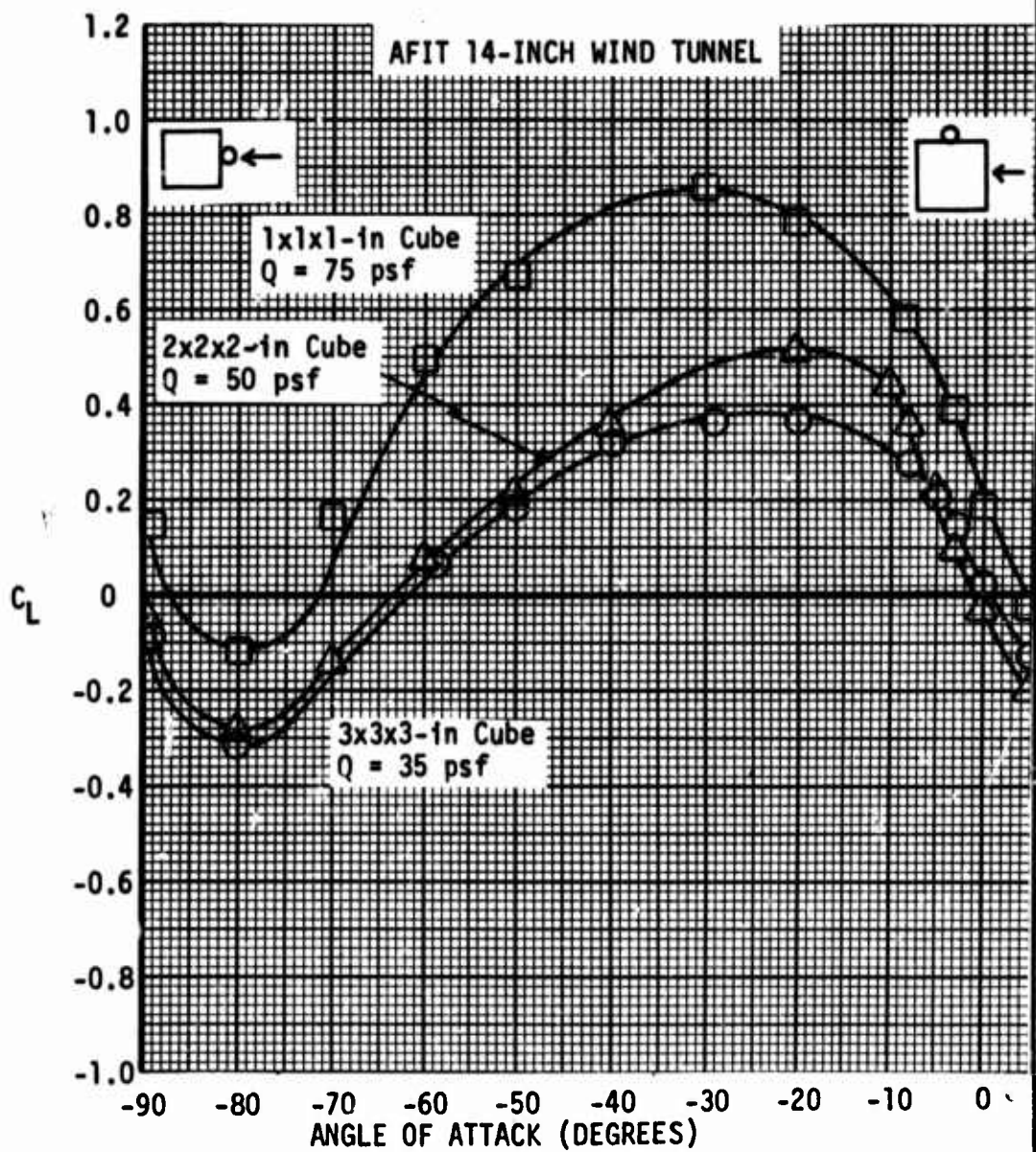


Fig. B.11. Lift coefficient vs angle of attack for cubes of various sizes.

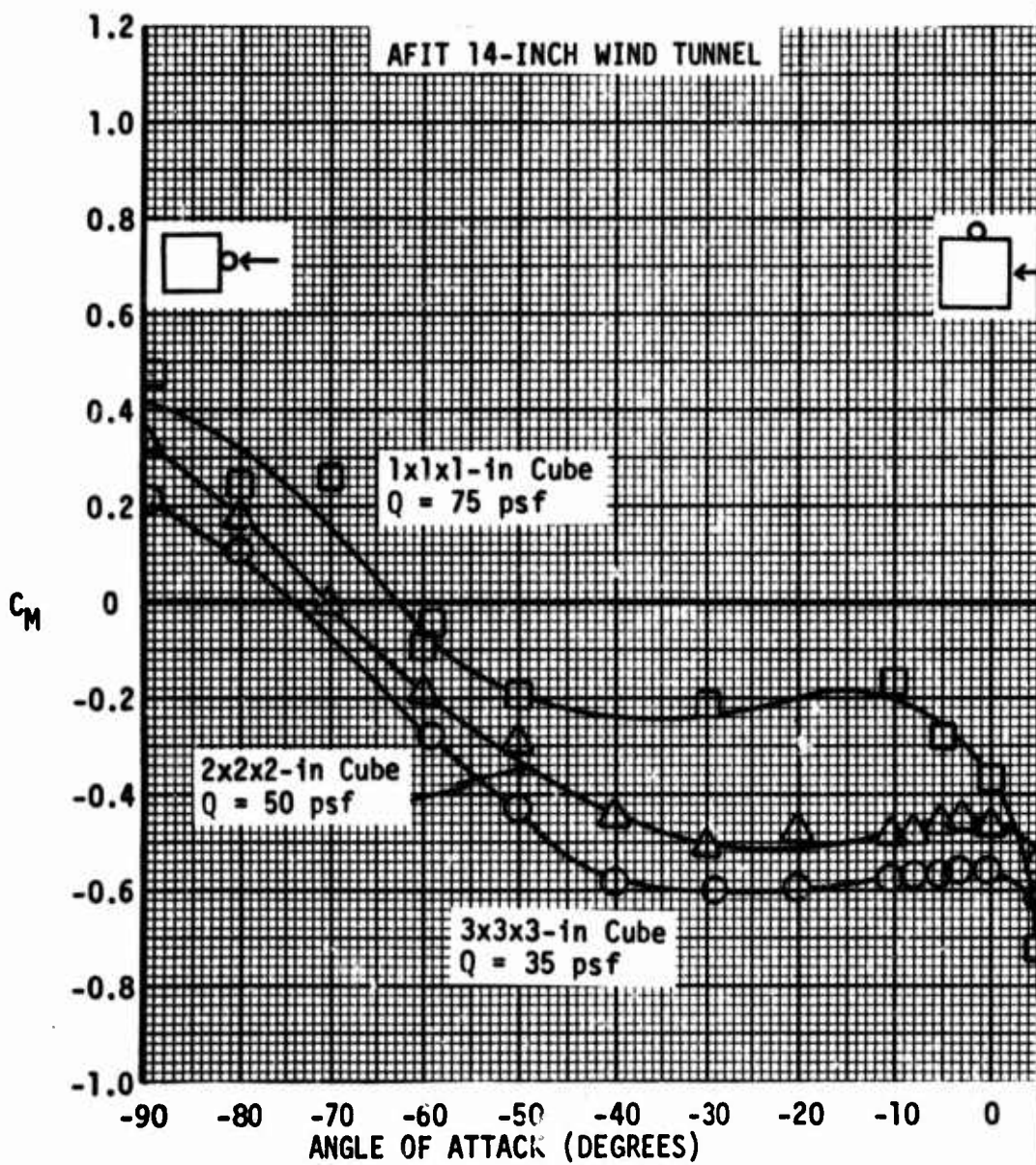


Fig. B.12. Pitching moment coefficient vs angle of attack for cubes of various sizes.

Appendix C

Sample Calculations

The wind tunnel data in this report have been reduced by methods described by A. Pope in his book Wind Tunnel Testing (Ref 3:337). The numbers used in the sample calculations are from the 2x2x2-in cube at 30° angle of attack and with the tunnel speed set at $Q = 50$ psf. All coefficients are based on model frontal area at 0° angle of attack.

Tunnel Blockage Factor

$$e = (MFA + SFA)/4C$$

$$e = (4 \sin 30^\circ + 4 \cos 30^\circ + 26.0)/4(150)$$

$$e = 0.0525$$

Corrected Dynamic Pressure

$$Q = Q_u(1 + 2e)$$

$$Q = 50[1 + 2(0.0525)]$$

$$Q = 55.25 \text{ psf}$$

Drag Coefficient

$$C_D = D/QS$$

$$D = 1.04[(D_s + I_m + D_m) - (D_s + I_m)]$$

Where $D_s + I_m + D_m =$ Net drag force from wind tunnel data

$D_s + I_m =$ Tare values from Fig. B.1.

1.04 = The slope of the drag calibration curve,
Fig. B.6.

I_m is assumed to be 0.

$$D = 1.04[4.51 - 2.56]$$

$$D = 2.03 \text{ lb}$$

$$C_D = 2.03/(55.25)(0.0278)$$

$$C_D = 1.325$$

Lift Coefficient

$$C_L = C_L [1 - \tau_2 \delta (S/C) (57.3) (a)]$$

$$C_L = L/QS$$

$$L = (L_s + I_m + L_m) - (L_s + I_m)$$

Where $L_s + I_m + L_m$ = Net force from wind tunnel data

$L_s + I_m$ = Tare values from Fig. B.2.

I_m is assumed to be 0.

$$L = (-0.29) - (0.30)$$

$$L = -0.59$$

$L = +0.59$ lb Since model was mounted inverted.

$$C_L = 0.59 / (55.25)(4.0/144)$$

$$C_L = 0.386$$

$$\tau_2 = 0.25 \text{ (Ref3.318)}$$

$$\delta = 0.125 \text{ (Ref3.297)}$$

$$C_L = 0.386 [1 - 0.25(0.125)(4.0/150)(57.3)(0.2/10)]$$

$$C_L = 0.385$$

The streamline curvature corrections were found to be small and have been neglected.

Pitching Moment Coefficient

$$C_m = M/QS l$$

$$M = (M_s + I_m + M_m) - (I_m + M_s)$$

Where $M_s + I_m + M_m$ = Net pitching moment from wind tunnel data

$M_s + I_m$ = Tare values from Fig. B.3.

l = Model length at 0° angle of attack

I_m is assumed to be 0.

$$M = (-1.35) - (-2.90)$$

$$M = +1.55$$

$$M = -1.55 \text{ in-lb Since model was mounted inverted.}$$

$$C_m = -1.55/(55.25)(0.0278)(2.0)$$

$$C_m = -0.506$$

Reynolds Number

$$R_n = \rho V l / \mu$$

$$T = 34^\circ\text{C} + 273$$

$$P = 29.098 \text{ in-hg}$$

$$Q = 55.25 \text{ psf}$$

$$\rho = \rho_o (P/P_o) (T_o/T)$$

$$\rho = 0.002378 (29.098/29.920) (288/307)$$

$$\rho = 0.00217 \text{ lb-sec}^2/\text{ft}^4$$

$$\mu = [358.3 + 0.987(^{\circ}\text{C})] 10^{-9}$$

$$\mu = [358.3 + 0.987(34)] 10^{-9}$$

$$\mu = (391.9) 10^{-9} (\text{lb-sec/ft})$$

$$V = \sqrt{2Q/\rho}$$

$$V = \sqrt{2(55.25)/(0.00217)}$$

$$V = 225 \text{ ft/sec}$$

$$l = 2/12$$

$$l = 0.1667 \text{ ft}$$

$$R_n = (0.00217)(225)(0.1667)/(391.9) 10^{-9}$$

$$R_n = 208,480$$

Appendix D

The following figures represent the lift, drag, and pitching moment coefficients versus angle of attack for rectangles and cylinders. The lift, drag, and pitching moment coefficient for a rectangle with various nose fairings is also shown.

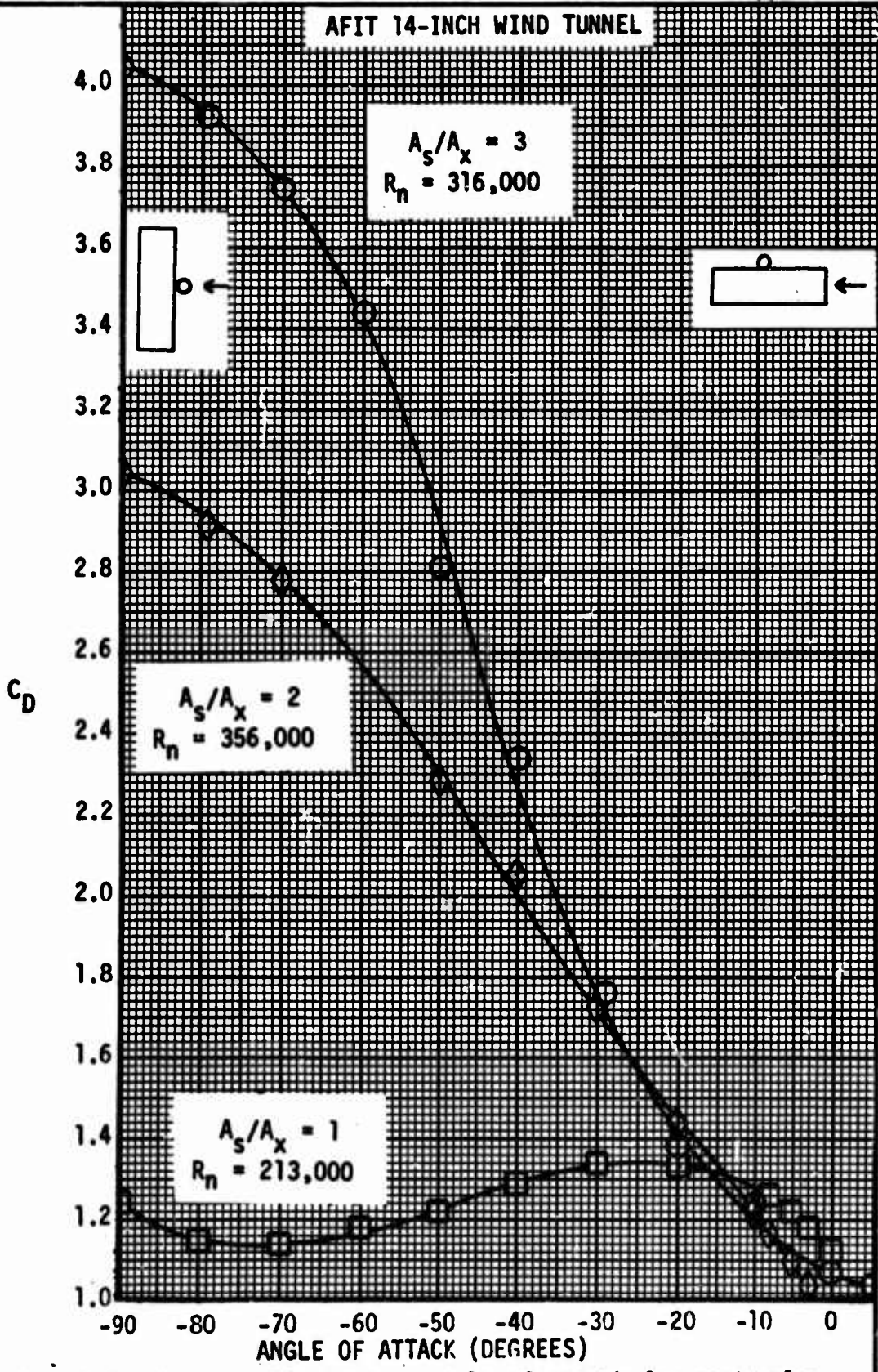


Fig. D.1. Drag coefficient vs angle of attack for rectangles at different ratios of side area to frontal area (A_S/A_X).

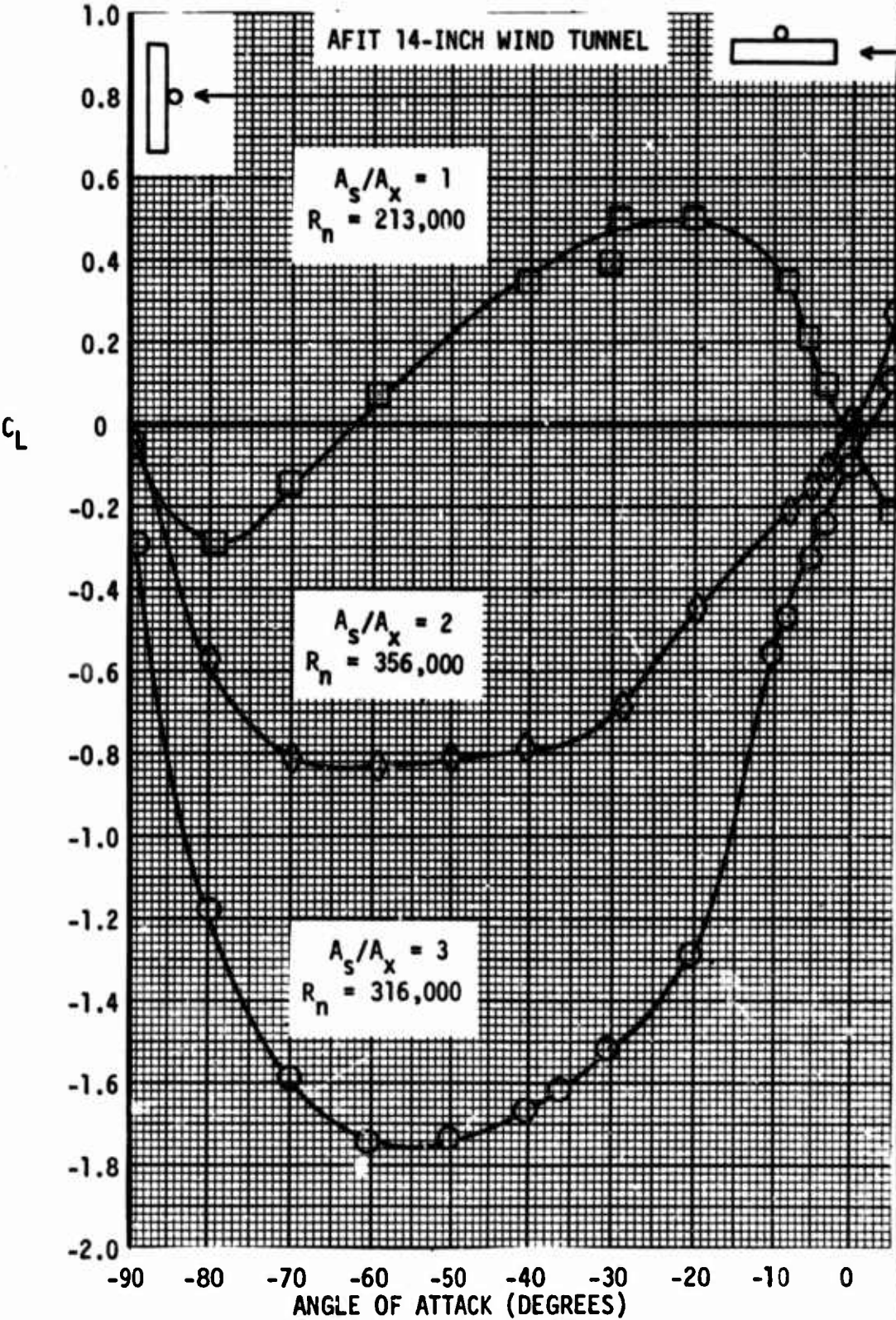


Fig. D.2. Lift coefficient vs angle of attack for rectangles at different ratios of side area to frontal area (A_S/A_X).

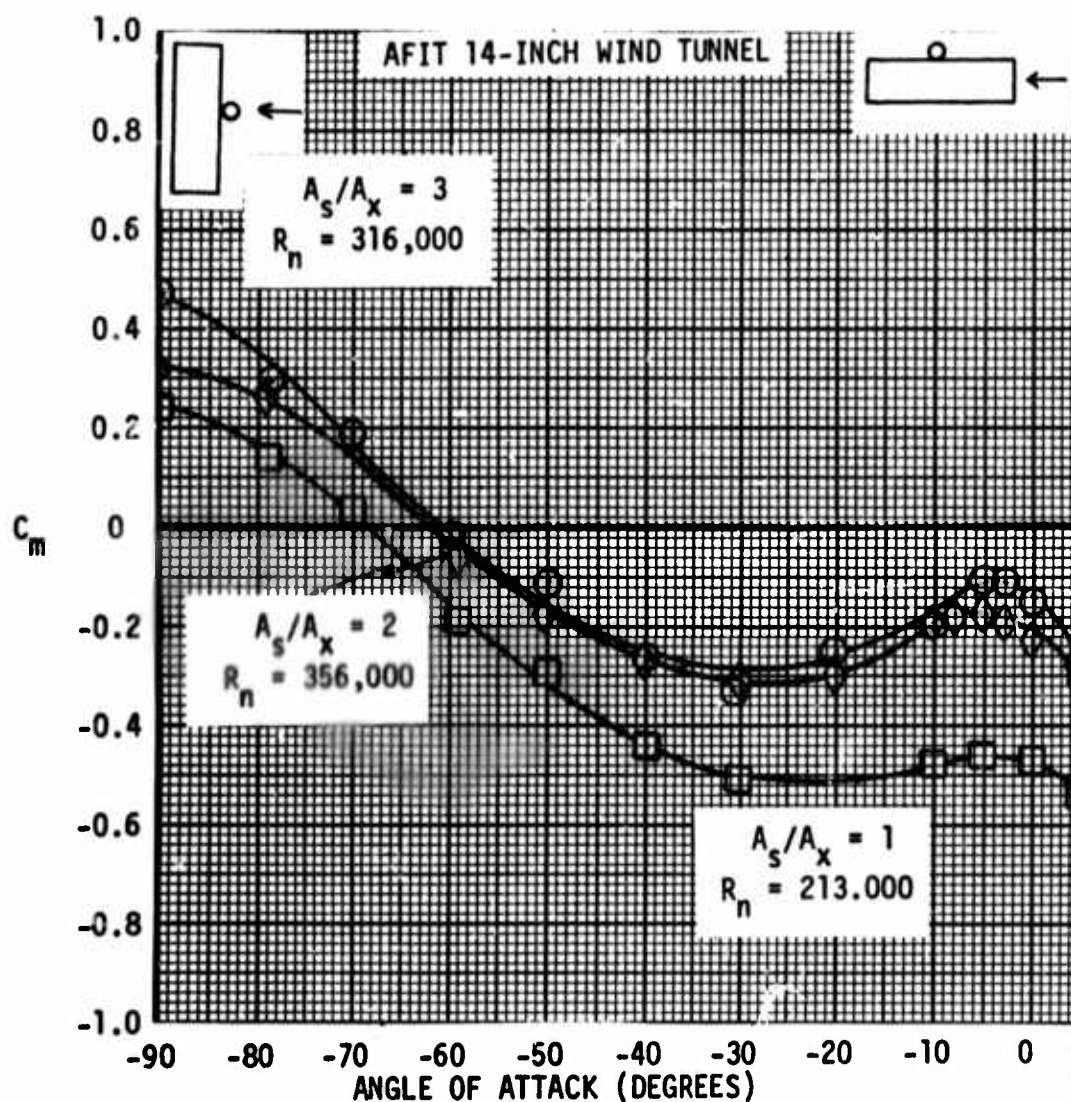


Fig. D.3. Pitching moment coefficient vs angle of attack for rectangles at different ratios of side area to frontal area (A_s/A_x).

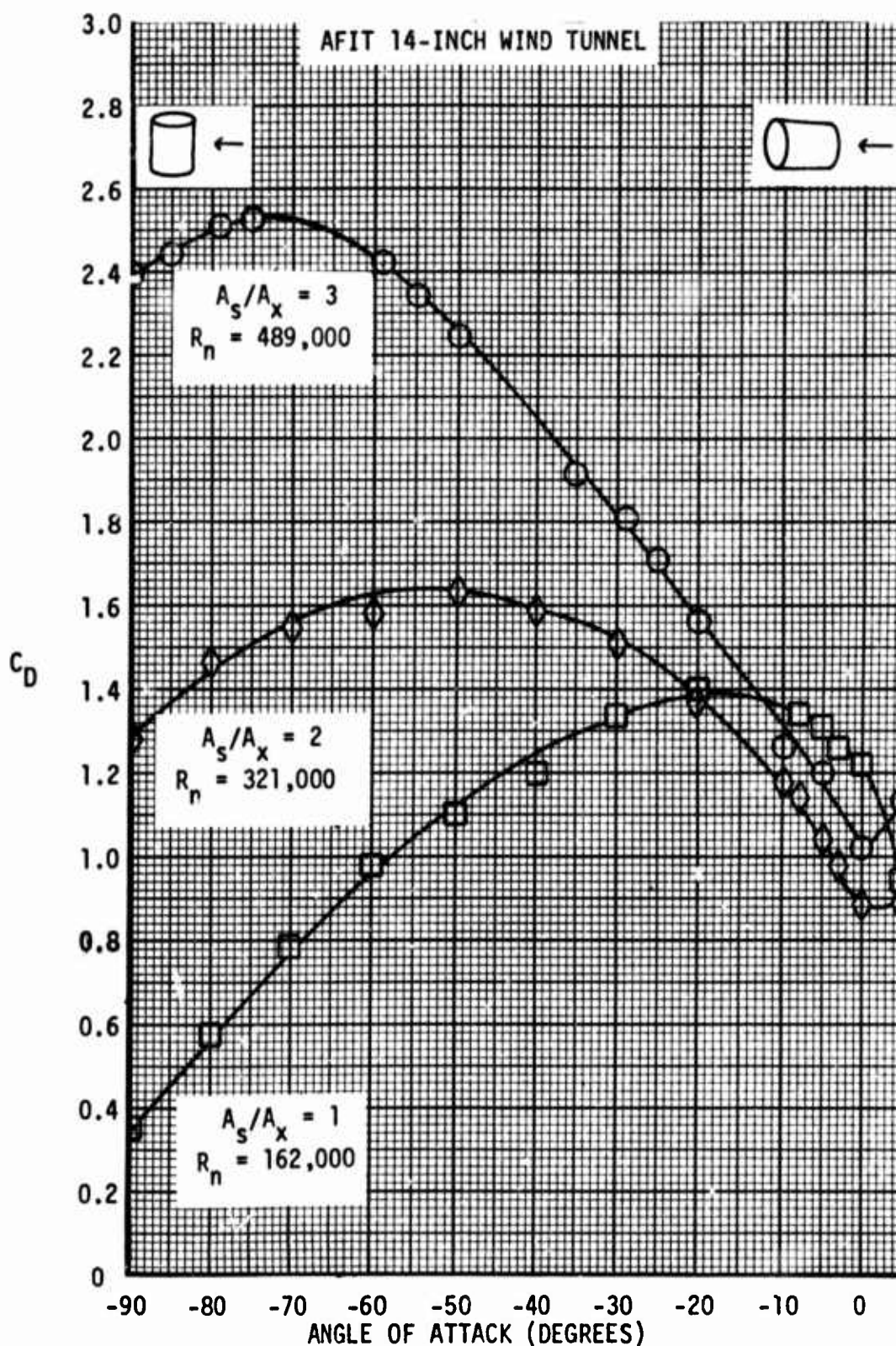


Fig. D.4. Drag coefficient vs angle of attack for cylinders at different ratios of projected side area to frontal area (A_s/A_x).

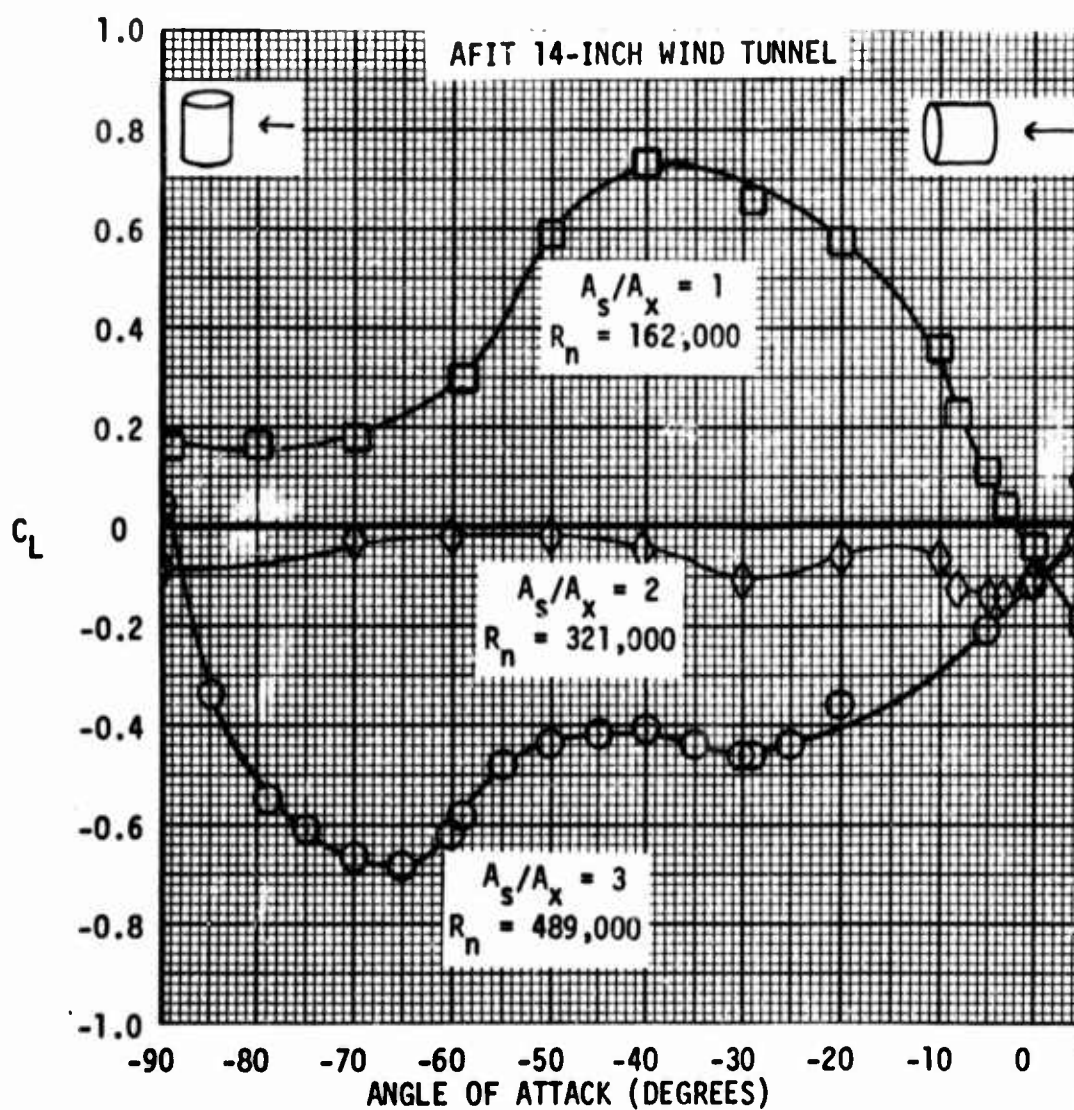


Fig. D.5. Lift coefficient vs angle of attack for cylinders at different ratios of projected side area to frontal area (A_s/A_x).

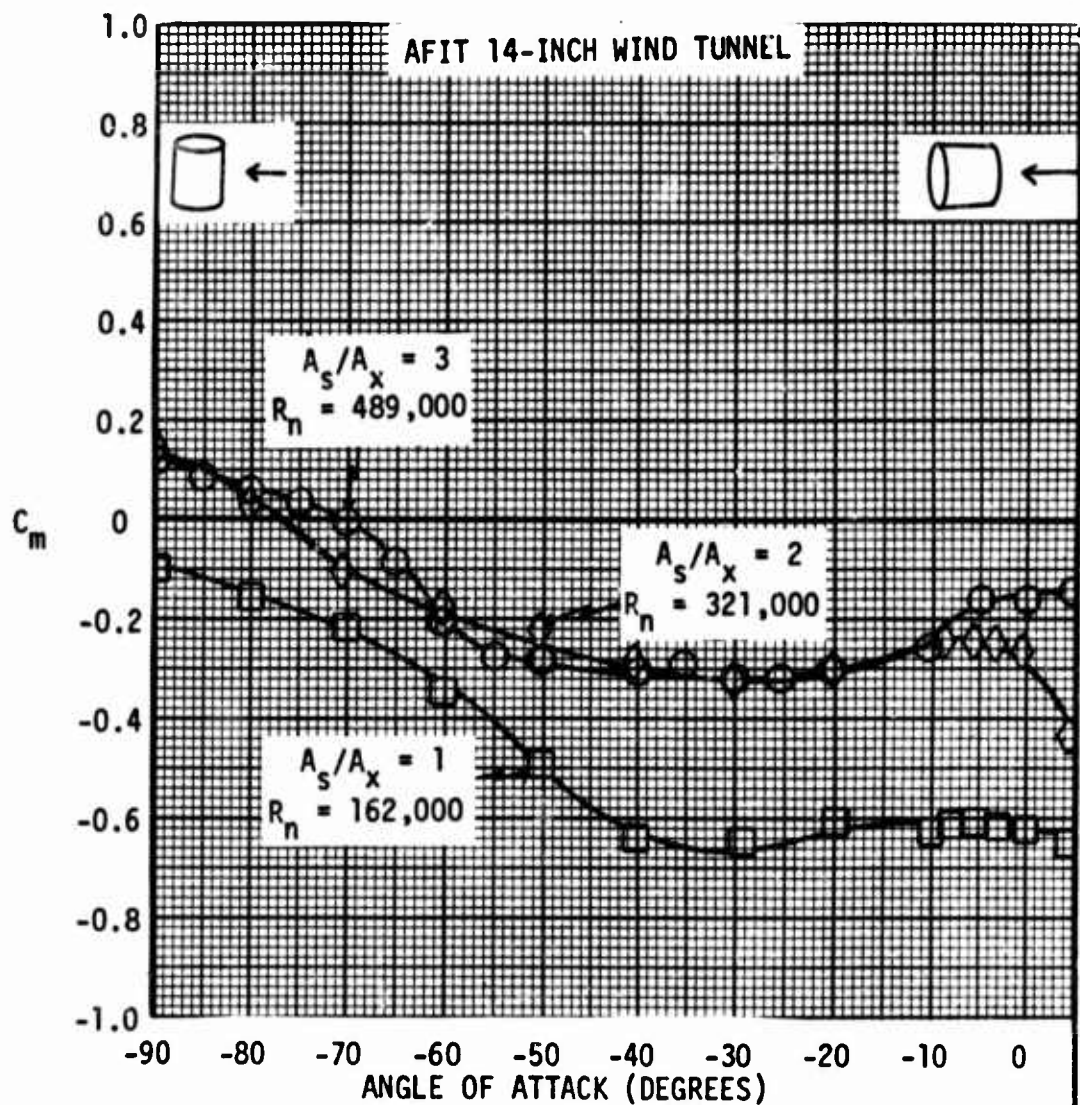


Fig. D.6. Pitching moment coefficient vs angle of attack for cylinders at different ratios of projected side area to frontal area (A_s/A_x).

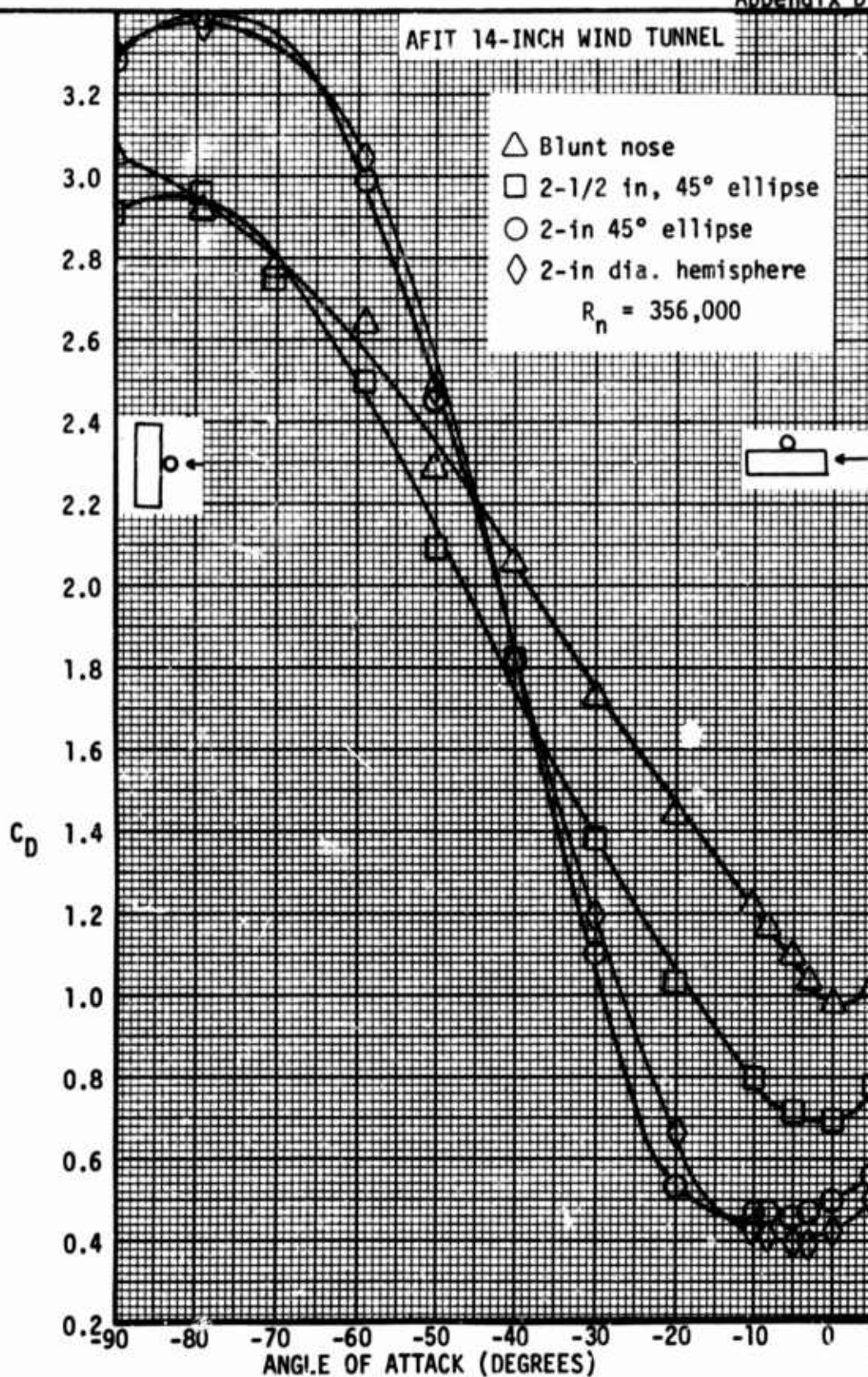
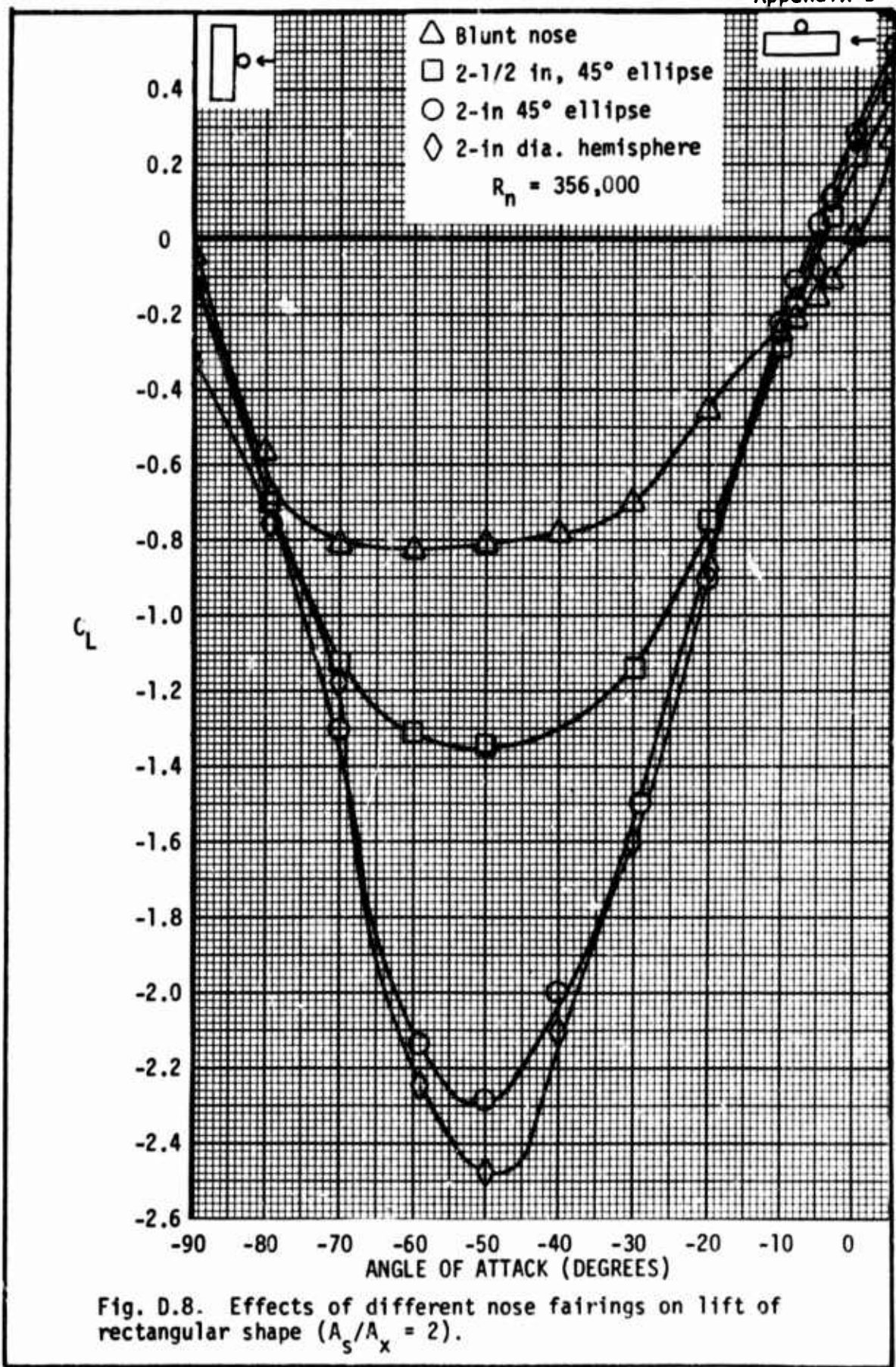


Fig. D. 7. Effects of different nose fairings on drag of rectangular shape ($A_s/A_x=2$).



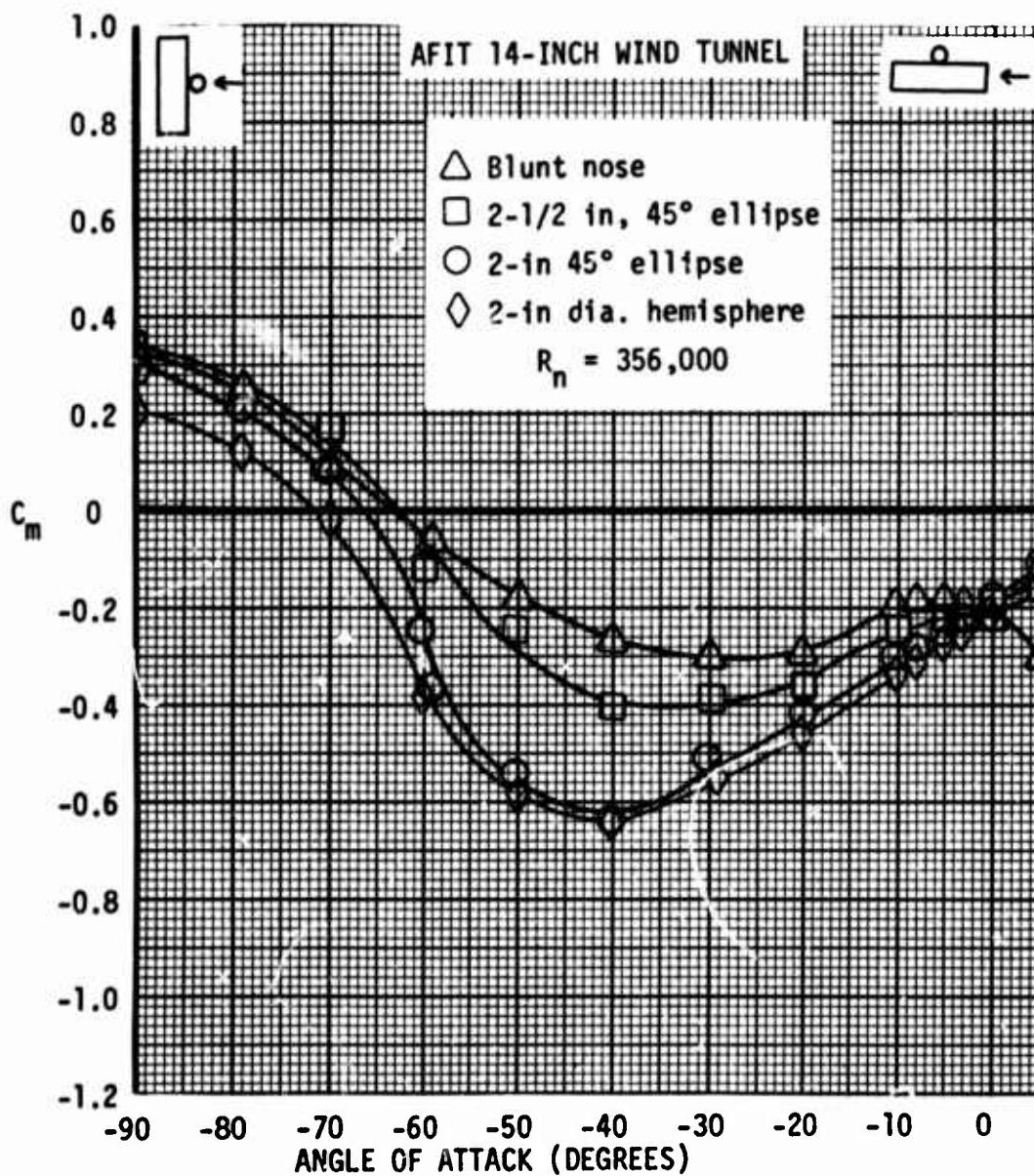


Fig. D.9. Effects of different nose fairings on pitching moment of rectangular shape ($A_s/A_x=2$).

VITA

Maurice John William Lehmann was born 1 April 1936 in Boerne, Texas. He graduated from Boerne High School in 1954 and attended the University of Texas where he received a Bachelor of Science degree in Aeronautical Engineering and a commission in the USAF in 1959. After attending flying school at Moore Air Base and Laredo Air Force Base, he was assigned to the 18th Military Airlift Squadron at McGuire Air Force Base, New Jersey, where he served as an aircraft commander and instructor pilot until entering the Air Force Institute of Technology.

Permanent address: Box 507

Boerne, Texas 78006

This thesis was typed by Mrs. M.J. Lehmann

UNCLASSIFIED

Security Classification

DOCUMENT CONTROL DATA - R & D

(Security classification of title, body of abstract and indexing annotation must be entered when the overall report is classified)

1. ORIGINATING ACTIVITY (Corporate author) Air Force Institute of Technology (AFIT-SE) Wright-Patterson AFB, Ohio 45433		2a. REPORT SECURITY CLASSIFICATION UNCLASSIFIED	
		2b. GROUP	
3. REPORT TITLE THE AERODYNAMIC CHARACTERISTICS OF NON-AERODYNAMIC SHAPES			
4. DESCRIPTIVE NOTES (Type of report and inclusive dates) AFIT Thesis			
5. AUTHOR(S) (First name, middle initial, last name) Lehmann, Maurice J.W., Capt., USAF			
6. REPORT DATE June 1968		7a. TOTAL NO. OF PAGES 54	7b. NO. OF REFS 7
8a. CONTRACT OR GRANT NO. b. PROJECT NO. N/A c. d.		9a. ORIGINATOR'S REPORT NUMBER(S) AFIT Thesis GAM/AE/68-6 9b. OTHER REPORT NO(S) (Any other numbers that may be assigned this report) N/A	
10. DISTRIBUTION STATEMENT This document is subject to special export controls and each transmittal to foreign governments or foreign nationals may be made only with prior approval of the Dean, School of Engineering, Air Force Institute of Technology (AFIT-SE), Wright-Patterson Air Force Base, Ohio 45433.			
11. SUPPLEMENTARY NOTES		12. SPONSORING MILITARY ACTIVITY Department of Aeronautical Engineering Air Force Institute of Technology (AFIT-SE) Wright-Patterson AFB, Ohio 45433	
13. ABSTRACT A wind tunnel investigation of three basic shapes (cubes, rectangles, and cylinders) was conducted to determine the aerodynamic characteristics of similar shaped cargos carried externally by helicopters or V/STOL aircraft. The ratio of side area to frontal area (A_s/A_x) was used as a parameter to plot the lift, drag, and pitching moment versus angle of attack for the three shapes. The lift, drag, and pitching moment coefficients were plotted for angles of attack from +5° to -90°. The change in slopes of the pitching moment of both rectangles and cylinders was smooth and gradual indicating no rapid changes in static stability. By using a very flat nose fairing (i.e., 10% of model length or less), it was possible to reduce the drag by 30% at 0° angle of attack without increasing the forces at the larger angles of attack.			

DD FORM 1 NOV 65 1473

UNCLASSIFIED

Security Classification

14. KEY WORDS	LINK A		LINK B		LINK C	
	ROLE	WT	ROLE	WT	ROLE	WT
Aerodynamic Characteristics Rectangles and Cylinders Nose Fairings Non-Aerodynamic Shapes External Cargo						